Thermal Science and Engineering Progress 20 (2020) 100679

Contents lists available at ScienceDirect

Thermal Science and Engineering Progress

journal homepage: www.elsevier.com/locate/tsep

Performance evaluation of external fired hybrid solar gas-turbine power plant in Colombia using energy and exergy methods

Faustino Moreno-Gamboa[a], Ana Escudero-Atehortua[b], César Nieto-Londoño[b,*]

[a] Facultad de Ingeniería, Grupo de Investigación FLUTER, Universidad Francisco de Paula Santander, Cúcuta, Colombia
[b] Escuela de Ingenierías, Universidad Pontificia Bolivariana, Medellín, Colombia

ARTICLE INFO

Keywords:
Thermosolar gas-turbine
Hybrid plants
Thermodynamic model
Variable solar irradiance
Global plant performance
Direct normal irradiance

ABSTRACT

Hydro and thermal generation power systems dominate the Colombian electricity sector. In 2017, Colombia installed electrical generation capacity was 16.8 GW. Renewable energy sources represent at least 85% of the total generation, being hydro the principal source. Several alternatives had been evaluated through the years to improve the Colombian energy matrix and capacity, including solar photovoltaic and wind plants; despite that, no consensus about the appropriate solution in terms of the available resource, energy demand, and energy mix has been attained. Thermosolar power plants arise as an alternative to produce energy in sites where nearly constant solar irradiance throughout the year is available, which is the case for most Colombian cities. This work concerned the evaluation of a single-stage hybrid Central Solar Power (CSP) plant at a location on the Caribbean Colombian coast. The study is focused on establishing the effect of local environmental conditions (ambient temperature and solar resource availability), as well as some operational cycle parameters (heat exchanger effectiveness and the system pressure ratio) on the CSP plant performance. Additionally, site emplacement conditions, i.e., proximity to the power grid, presence of conventional thermal power plants, proximity to principal cities, and availability of natural gas), are also considered to attain the factors that might constrain the plant optimal operating conditions. The CSP plant and the Direct Normal Irradiance (DNI) model results obtained fitted in good agreement the experimental data from the literature used for validation. Results have shown a global plant efficiency of 35% without solar resource which is reduced to 30% when solar contribution attains its maximum value at midday. Additionally, fuel-saving per day varies between 9.21% and 6.3% during the months of maximum and minimum global radiation, respectively. Finally, that the combustion chamber, its associated heat exchanger and the one that is in direct exchange with the surroundings, are the components with the most exergy destruction, as expected. From the above, it is sensible to explore alternatives regarding different working fluids that could be used in lower temperature cycles and other applications for heat recovery.

1. Introduction

The Colombian electrical sector is mainly supported on hydropower and thermoelectric plants, dispatched trough the National Interconnected System (SIN for the Spanish acronym) [1]. With an installed capacity of 16.8 gigawatts (GW) by 2017, Colombian electrical generation system has a share of 69.85% of hydropower and 29.02% of thermal power plants [2]. The remaining 1% corresponds to non-conventional renewable sources (i.e., solar PV and wind), Combined Heat and Power and self-generation plants, as shown in Fig. 1. Hydropower generation supply to the SIN increased by 21% for 2017 compared to the previous year. Meanwhile, thermal power decreased by 55.4% for the same period, coinciding with the end of the longest “el Niño” event since 1950 [3].

The electricity demand in Colombia is expected to increase above 37% between 2015 and 2030 [1]. To cope that, the Colombian government had proposed renewable energy policies aiming the implementation of alternative energy sources and its incorporation into the energy market [4]. Despite this kind of initiatives and the country’s renewable energy potential, hydro and thermal power plants dominate current electrical expansion plans, with a recently growing interest in the implementation of solar photovoltaic and wind power plants [5]. Hydropower dominance is the result of low energy costs and high hydro potential in the country. However, the construction of large dams carries a significant environmental footprint because reservoirs modify the river’s ecosystem. On the other side, thermoelectric plants energy costs dominated by fuel prices volatility, and at the same time, are a growing source of Greenhouse Gases despite some efforts to use alternative fuels

* Corresponding author.
E-mail address: cesar.nieto@upb.edu.co (C. Nieto-Londoño).

https://doi.org/10.1016/j.tsep.2020.100679

Available online 14 August 2020

Nomenclature

$\overline{D}_h$	Monthly average daily diffuse solar irradiance, kWh/m^2/day
$\overline{H}_h$	Monthly average daily global solar irradiance, kWh/m^2/day
$\dot{E}_{d,a}$	Exergy destruction in the ambient heat exchanger, kW
$\dot{E}_{d,cc}$	Exergy destruction in the combustion chamber, kW
$\dot{E}_{d,c}$	Exergy destruction in the compressor, kW
$\dot{E}_{d,he}$	Exergy destruction in the heliostat field, kW
$\dot{E}_{d,re}$	Exergy destruction in the central receptor, kW
$\dot{E}_{d,r}$	Exergy destruction in the regenerator, kW
$\dot{E}_{d,t}$	Exergy destruction in the turbine, kW
$\dot{E}_{x,i}$	Inlet exergy to central receptor, kW
$\dot{E}_{x,s}$	Inlet exergy to the solar concentrator, kW
$\dot{m}$	Mass flow rate of the working substance, kg/s
$\dot{m}_f$	fuel mass flow rate, kg/s
$\dot{Q}_h$	Total heat-transfer rate absorbed from the working fluid, kW
$\dot{Q}_l$	Heat rate loss to surroundings in central receptor, kW
$\dot{Q}_p$	Heat rate loss in central receptor, kW
$\dot{Q}_r$	Heat rate input to central receptor, kW
$\dot{Q}_{hct}$	Heat rate input to heat exchanger from combustion chamber, kW
$\dot{Q}_{hc}$	Heat input from the combustion chamber, kW
$\dot{Q}_{hst}$	Heat rate input to heat exchanger from central receptor, kW
$\dot{Q}_{hs}$	Heat input from solar collector, kW
$\dot{W}_c$	Power inlet compressor, kW
$\dot{W}_t$	Power output turbine, kW
$\dot{W}_{net}$	Power net output, kW
η	Overall energy efficiency
η_0	Optical efficiency
η_c	Isentropic efficiency of the compressor
η_h	Thermal efficiency of the Brayton heat engine
η_t	Isentropic efficiency of the turbine
η_{exh}	Exergy efficiency of the Brayton heat engine
η_{ex}	Overall exergy efficiency
ε_l	Heat exchanger surrounding effectiveness
ε_r	Regenerator effectiveness
ε_{ic}	Combustion chamber heat exchanger effectiveness
ε_{is}	Solar receptor heat exchanger effectiveness
A_o	Heliostat field area, m^2
A_r	Area of incidence in the central receiver, m^2
D_{pi}	Irreversibilities due to pressure drops in the heat input
D_{ps}	Irreversibilities due to pressure drops in the heat output
f	Solar share
$F\dot{E}_{d,j}$	Exergy destruction fraction for component
h	Specific enthalpy, kJ/kg
I_h	Global solar radiation, W/m^2
I_{bh}	Diffuse solar radiation, W/m^2
I_{bh}	Direct solar radiation, W/m^2
LHV	Lower heating value of the fuel, kJ/kg
r_d	Hourly to daily ratio for diffuse radiation
r_e	Fuel conversion rate
r_p	Overall pressure ratio
r_tg	Ratio of hourly radiation to the total daily radiation
s	Specific entropy, kJ/kgK
T_{hc}	Working temperature of the combustion chamber, K
T_{hs}	Working temperature of the solar collector, K
U_L	Conduction–convection heat transfer coefficient, W/m^{2}K

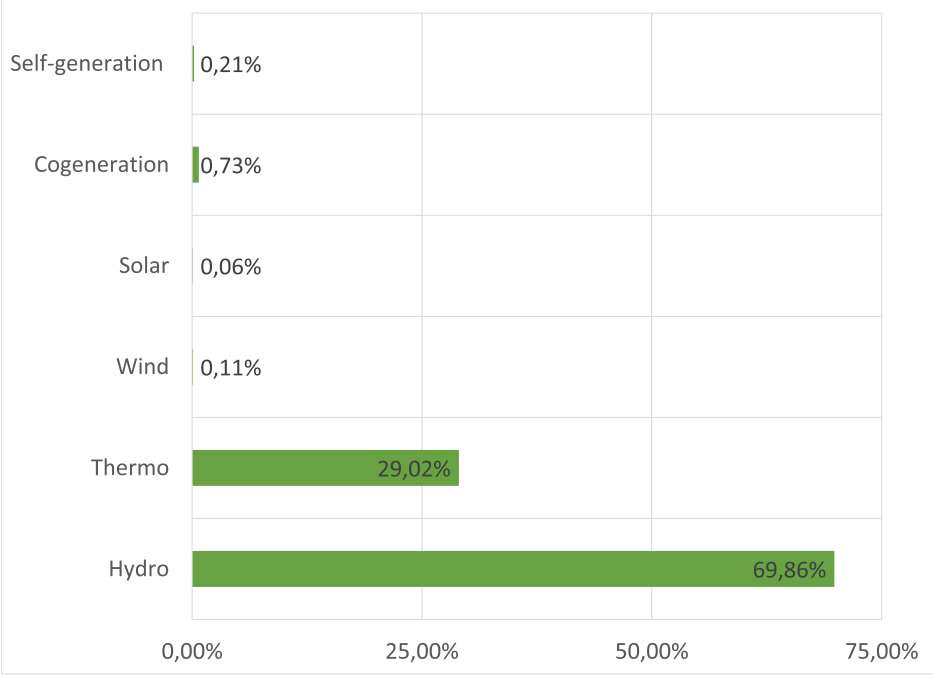

Fig. 1. Composition of installed electricity generation capacity in Colombia in 2017 [3].

[6].

Concentrated Solar Power (CSP) plants have gained attention in the last years as an alternative to reduce fossil fuel consumption for electricity generation, increase power generation and its associated environmental impact, among others [7–9]. Installed solar thermal capacity worldwide rose from 1.1 GW in 2011 to 4.8 GW by 2015, representing a 436% growth in just four years [6]. However, the commercial interest in these plants is limited to their higher Levelized Cost of Electricity (LCOE) when compared with conventional power generation systems [10]. Efforts in this regard are deemed essential to

the study of efficient thermodynamic power cycles to increase its performance to get more significant power production with reduced fuel consumption, and therefore, decreasing emissions and eventually costs [11–13].

Different approaches focused on studying the coupling of Brayton cycles and CSP plants to improve its performance, define future configurations, and evaluate the effect of different working fluids on the overall efficiency [14,15]. In this regard, other works have developed the analysis of arrangements that allow increasing availability of CSP plants using thermal storage [16] Thermal storage are a first solution for energy utilisation to fill the gap between demand and supply to improve the energy efficiency of this kind of systems. Alternatives for thermal energy storage include sensible heat storage, latent heat storage, thermochemical energy storage, and phase change materials heat storage [17]. Recovering waste heat can be also implemented regarding the efficiency of the system through various waste heat recovery technologies to provide valuable energy sources and to reduce the overall energy consumption [18]. Other works suggest that solar energy collection can be improved by using magnetic nanofluids [19]. Conversely, hybridization of CSP plants are an alternative for its operation during null or low solar irradiance as a substitute for thermal storage, in particular for those based on Brayton cycles [20]. In this aim, Gas Turbine (GT) plants have a wide range of advantages when compared with Steam Turbine (ST) power plants, showing a more compact configuration, and the possibility to use fewer water requirements. Additionally, GT has demonstrated significant improvements in efficiency to reduce fuel consumption [21]. Besides, GT plants can be integrated with CSP plants [10], with tower and central receiver systems operating at higher temperatures and improving its efficiency [22,23].

Small combined cycle plants with solar concentration systems could be used in industrial or residential sectors [24]. Thermosolar power has also been proved to use in greener ammonia synthesis utilising hydrogen produced from solar thermal cracking of methane [25]. Nakatani and Osada [26] presented the evaluation of integrating small gas turbines with a central tower concentration system with heliostats achieving temperatures at the central receiver output greater than 850 °C. Meanwhile, Kin et al. [27] performed a parametric study and optimisation of closed Brayton power cycle considering variations in the charge amount of working fluid. The results of this study allow concluding that the charge amount must be used as a control parameter during the design and operation of closed Brayton cycles.

Thermo-economic analysis of existing CSP systems considering the integration with combined cycles [28] and the use of evolutionary algorithms for its optimisation [29] are significant approaches to the development of these plants. Life Cycle Models were used to estimate CSP system costs being, the heliostats field and the combustion chambers and boilers the subsystems with the highest impact in the overall system cost [30]. Annual performance, fuel consumption and emissions of a hybrid thermosolar central tower Brayton plant is analysed in [31] by means of a thermodynamic model, where subsystem models consider all the primary irreversibility sources existing in real installations. As results, it is observed that any improvement in the Brayton heat engine efficiency, will conduce to an increase of performance on the overall thermal efficiency. Additionally, a hybrid Brayton thermosolar tower power plants study for different fluids and plant configurations is analysed in [32], including main energy losses in each plant subsystem for some particular plant layouts. Results showed that specific carbon dioxide emissions are smaller for the plant operating with helium when compared with dry air, both working in a single-stage non-recuperative closed cycle.

Most of the CSP plants with Brayton cycles reported in the literature are composed of one compression and expansion stage [33] or at most, a combination of one or two compression or expansion stages as described by Behar [34]. Additionally, thermoelectric solar power plant studies have been carried out with solar radiation data measured for the city of Seville, Spain, in which the operation of the plant has been evaluated for typical days during the four local seasons [35]. Thermodynamic models have also been developed for energy analysis of solar gas turbines with arbitrary numbers of compression and expansion stages [36]. Simulated values for heat losses due to radiation and convection in central towers showed deviations between 5.4% and 16.2% compared to experimental data [37].

A general thermodynamic model for an irreversible solar Brayton cycle considering heat loss at the receiver was used to determine the temperature operation and the overall efficiency of the cycle [38]. In other studies, system irreversibilites were considered, such as those due to heat transfer within the Joule-Brayton cycles to determine optimal operating conditions [39]. Heat losses are a significant concern for the design and operation of CSP power plants due to the higher temperatures attained in some components of the cycle. Thermodynamic models had been used to predict the effect of the airflow and parabolic trough collector's temperature on CSP plants performance [40]. These models had also been used to predict the impact of minor geometric modifications over the plant performance. For instance, the heat transfer improvement to the working fluid as a consequence of adding fins to the receiver tubes, implied an increase in the receiver's efficiency up to 91.5% [41]. Some other authors had evaluated the use of reheating methods over the system efficiency [42]. In the same direction, entropy minimisation models had been used to explore strategies to reduce losses due to high heat transfer rates at the concentrator [43]. Small-scale Brayton cycle plant optimisation using air as working fluid included heat loss at the receiving open cavity coupled to the collector's plate [18] and the study over the efficiency of the open cavity with an inner tube and the plant operation [44].

In [45] a multi-objective optimisation study of simple closed Brayton cycle with one isothermal heating process is presented. For the optimisation, the dimensionless power density is used as the optimisation objective. Additionally, the effects of inlet temperature ratios of combustion chambers on the optimal performances are analysed. Results show that adding a convergent combustion chamber to the cycle can increase the dimensionless power density by 18.57%. An optimisation of a super-critical carbon dioxide Brayton cycle is presented in [46]. The pressure ratio and the flow split fraction were examined for sensitivity analysis and optimisation of the cycle. The study showed that the cycle thermal efficiency was improved by changing the channel shape due to a reduction in heat exchanger's pressure drop. A closed-loop, indirect, super-critical Carbon Dioxide (sCO2) power cycle for fossil-fuel, solar thermal and nuclear applications is presented in [47], where its ability to achieve higher efficiency and compactness is studied. Optimisation of the whole plant was performed being the pressure ratio the design variable. Results indicate that the sCO2 Brayton cycle considered, attained maximum plant efficiency at a different GT pressure ratio. It was also probed that the optimum GT pressure ratio to realise the maximum cost reduction in sCO2 cycle is higher when compared to the equivalent steam Rankine cycle.

Regarding the study of solar plants by using exergy approaches, in [48] an exergo-economic analysis and optimisation of a solar double pressure organic Rankine cycle is presented. Exergo-economic criteria revealed that solar collector has the most value of exergy destruction and high investment costs of the collector. Exergy analysis have been also explored to estimate that a parabolic trough concentrator destroys close to 70% of the total plant exergy [49]. On the other side, Zare and Hasanzadeh [50] present an energy and exergy study of a solar plant with helium and organic bottoming cycle. Additionally, an exergy analysis of a super-critical hybrid carbon dioxide central tower solar plant for different locations in Saudi Arabia [51] presents that the most considerable destruction of exergy occurs in the field of heliostats and the combustion chamber. Ahmadi et at [52] done a thermodynamic study of a small-scale trans-critical CO2 power cycle. They used a flat plate collector and a storage tank as a heat source and liquefied natural gas (LNG) as the heat sink. Results showed that condensation temperature has a significant effect on the performance of the system;

however, the system efficiency and the net power output are less sensitive to the change in inlet temperature of the turbine. Other, exergy models for Brayton plants with different heat sources, including conventional systems and renewable systems, have been developed [53], showing that most significant exergy destruction occurs in the combustion chamber and is reduced with the addition of heat sources at a lower temperature. Some of the latest studies of super-critical carbon dioxide cycles included the evaluation of technical and economic aspects [54].

Regarding the study of alternatives for the Colombian's energy mix diversification, this paper presents the performance evaluation of a hybrid solar central thermal power plant at a location on the Caribbean Colombian coast considering local environmental conditions such as ambient temperature and solar resource availability. The Brayton CSP hybrid plant is composed of a central tower plant, a heliostats field, and an external combustion chamber that ensures the power production during low or nil solar resource contribution. First and second law balances are used to quantify the effect of ambient temperature and irradiation conditions for a location in Colombia over a specific day to establish the corresponding impact on CSP energy and exergy efficiencies. The exergy destruction and the influence of the pressure ratio of the plant are alos evaluated. The plant models and thermodynamic properties of the working fluid are assessed using the Modelica [55] compiler Dymola ® [56]. Air properties at any cycle states are estimated with the DryAirNASA model from the *Modelica. Media. Air* library using the definition of each state from two thermodynamic properties, enthalpy (h) pressure (p), temperature (T) or entropy (s) [57,58].

The document is organized as follows: Section 2 describes the models used in this work, beginning with the solar radiation model that allows finding a daily distribution of the Direct Normal Irradiance (DNI). Then, the thermodynamic model for the hybrid solar closed Brayton cycle is depicted, including irreversibilites accounted in the process. The exergy destruction models for each system component are also described in section Section 2. Section 3 presents the solar radiation model validation, using data reported in the literature for a plant with similar conditions. Then, the simulated plant results for the Colombian conditions are shown in Section 4, including thermal efficiency and power produced, where pressure ratio variations are included to estimate optimal operating conditions. In Section 5, the exergy evaluation of each component is presented. Finally, Section 6 comprises the conclusions of this work.

2. Model and plant configuration

This section describes the DNI model used for the evaluation of solar irradiation regarding Colombian conditions. The CSP plant scheme with a Brayton Cycle is presented, as well as the thermodynamic models used for the energy and exergy analysis.

2.1. Solar radiation model

Evaluation of solar concentration system under specific irradiation site conditions require access to the Direct Normal Irradiance of the emplacement site. In the case of Colombia, those values are not publicly accessed. Since this information is fundamental to design and simulate concentrating solar system [57], a DNI model is required to predict the irradiance behaviour through the day. Daily average values and global diffuse solar radiation are used to obtain hourly data during a specific day of the month; from these values, the hourly distribution DNI is determined following the model proposed by Liu and Jordan [59]. Among the models that evaluate hourly radiation, the daily integration model developed by Gueymard [57] was designed to predict the monthly average global hourly radiation and was validated with data from 135 weather stations. This model is considered the most accurate after being compared and verified against others already developed and validated models [60,61] since it includes atmospheric attenuation introduced through time angles allowing a better prediction [62]. The total radiation on a horizontal surface, I_h, is defined as the sum of its components: direct radiation I_{bh} and diffuse radiation I_{dh}; therefore, direct radiation is defined as:

$$I_{bh} = I_h - I_{dh}, \tag{1}$$

where the hourly daily ratios for diffuse r_d and global radiation r_{tg}, are defined as,

$$r_d = \frac{I_{dh}}{\overline{D_h}}, \tag{2}$$

and,

$$r_{tg} = \frac{I_h}{\overline{H_h}}, \tag{3}$$

being D_h and H_h the long-term average daily total and diffuse irradiation on a horizontal surface, respectively. These values can be obtained from the National Aeronautics and Space Administration (NASA) [63] and are calculated using twenty years of analysed data. Direct radiation is a function of daytime, and can be defined in terms of the global and diffuse radiation, as

$$I_{bh} = r_{tg}\overline{H_h} - r_d\overline{D_h} \tag{4}$$

where the relation r_d is obtained according to [60], as

$$r_d = \frac{\pi}{t}\frac{\cos\omega - \cos\omega_s}{\sin\omega - \sin\omega_s}, \tag{5}$$

where ω_s is the sunrise angle for a given day, ω the solar hour angle along the same day estimated according to the methodology proposed by Goswami [58] and t the time. The daily average extraterrestrial irradiation on a horizontal surface, H_o, is estimated as:

$$H_o = \frac{24}{\pi}\omega_s R E_{sc}\sin h_o \tag{6}$$

being E_{sc} the solar constant (1367 W/m^2) and $R = (D_o/D)^2$, the average sun-earth correction factor; D is the distance between the sun and the earth, which varies according to the location of the planet according to the elliptical orbit around the sun. D_o is the average annual distance between the sun and the earth estimated at 1.496×10^{11} m. This correction factor is estimated as,

$$R = 1.00011 + 0.034221\cos x + 0.00128\sin x + 0.000719\cos 2x + 0.000077\sin x, \tag{7}$$

where x is defined as,

$$x = \frac{360(n-1)}{365.242}, \tag{8}$$

and h_o is the daily average solar elevation outside of the atmosphere and is solving the following system,

$$\sin h_o = \frac{qA(\omega_s)}{\omega_s}, \tag{9}$$

$$q = \cos L\cos\delta, \tag{10}$$

and,

$$A(\omega_s) = \omega_s(\sin\omega_s - \cos\omega_s), \tag{11}$$

where L is the latitude of the site for which the solar resource is being evaluated, and δ is the declination, according to [58]. The average clarity index K_t is defined as:

$$K_t = \frac{\overline{H_h}}{H_o}, \tag{12}$$

while the number of sun hours during the day S_o, is

$$S_o = \frac{24}{\pi}\omega_s. \tag{13}$$

The ratio of the horizontal hourly radiation to the total horizontal daily radiation r_{tg}, is obtained as follows,

$$r_{tg} = r_d \frac{1 + q\frac{24}{\pi}\frac{a_2}{a_1}A(\omega_s)r_d}{1 + q\frac{a_2}{a_1}\frac{B(\omega_s)}{A(\omega_s)}}, \tag{14}$$

where, a_1, is estimated as,

$$a_1 = 0.41342K_t + 0.61197K_t^2 - 0.01886K_tS_o, \tag{15}$$

and a_2 corresponds to the maximum value between 0.054 and the value calculated with,

$$a_2 = 0.28116 + 2.2475K_t - 1.7611K_t^2 - 1.84535\sin h_o + 1.681\sin^3 h_o \tag{16}$$

Finally, $B(\omega_s)$ is obtained as,

$$B(\omega_s) = \omega_s(0.5 + \cos^2\omega_s) - 0.75\sin 2\omega_s \tag{17}$$

2.2. Hybrid solar plant configuration and energy model

The thermodynamic analysis of the CSP plant carried out in this work is based on the scheme shown in Fig. 2. It consists of a closed cycle that uses air as working fluid. Air is compressed (Process 1–2) and expanded at the turbine (Process 5–6); both compressing and expansion processes are considered under adiabatic and irreversible conditions. Then, heat is recovered at constant pressure from air exiting the turbine and transfer through the regenerator to the working fluid, increasing its enthalpy at the compressor exit (Process 2–3). Next, the solar receiver (Process 3–4) concentrates the irradiation from the heliostats field and delivers heat to the air passing through a heat exchanger. To ensure continuous operation through the day, a combustion chamber (Process 4–5) burns natural gas and delivers heat to the air by another heat exchanger. Formerly, the air enters the turbine (Process 5–6), where the power is obtained. After the regenerator, a heat exchanger rejects heat to the surroundings (Process 1–6), regulating the temperature at the compressor inlet.

Fig. 3 shows the T-s cycle diagram of the closed solar thermal plant shown in Fig. 2. The heat $\dot{Q}_{hs}$ is supplied from the solar concentration system (Process 3–4), $\dot{Q}_{hc}$ is the heat supplied at the combustion chamber (Process 4–5) and $\dot{Q}_h$ is the residual heat released from the system to the surroundings at a temperature T_0 (Process 7–1). Heat exchangers present a pressure drop Δ_{ps} for the heat supply (Process 2–5) and Δ_{pi} for the heat rejection (Process 6–1).

The energy balance at the compressor can be expressed as follows,

$$\dot{W}_c = \dot{m}(h_2 - h_1), \tag{18}$$

being $\dot{W}_c$ the compressor power and $\dot{m}$ the air mass flow rate. The global pressure ratio for the cycle, r_p, and the pressure ratio for the compressor, r_c, are defined as,

$$r_c = r_p = \frac{P_{2s}}{P1} \tag{19}$$

where the isentropic efficiency of the compressor is as follows,

$$\eta_c = \frac{h_{2s} - h_1}{h_2 - h_1} \tag{20}$$

being h_i the enthalpy at each state and h_{2s} the enthalpy of the isentropic compression process. The regenerator transfers heat to the air exiting the compressor, from heat recovered at the turbine exit when $T_6 > T_2$ limited by the regenerator effectiveness as follows:

$$\varepsilon_r = \frac{h_3 - h_2}{h_6 - h_2} = \frac{h_7 - h_6}{h_2 - h_6} \tag{21}$$

The energy balance of the turbine is defined as,

$$\dot{W}_t = \dot{m}(h_6 - h_5), \tag{22}$$

where $\dot{W}_t$ corresponds to the work developed by the turbine at a determined turbine pressure ratio, r_t, defined as

$$r_t = D_{ps}D_{pi}r_p = \frac{P_5}{P_6}, \tag{23}$$

with an isentropic efficiency, η_t, expressed as

$$\eta_t = \frac{h_6 - h_5}{h_{6s} - h_5}. \tag{24}$$

As mentioned before, pressure losses Δ_{ps} and Δ_{pi} are considered in the heat exchangers during processes 2–5 (heat supply) and 6–1 (heat loss), respectively; then, lines representing the deviation from ideal

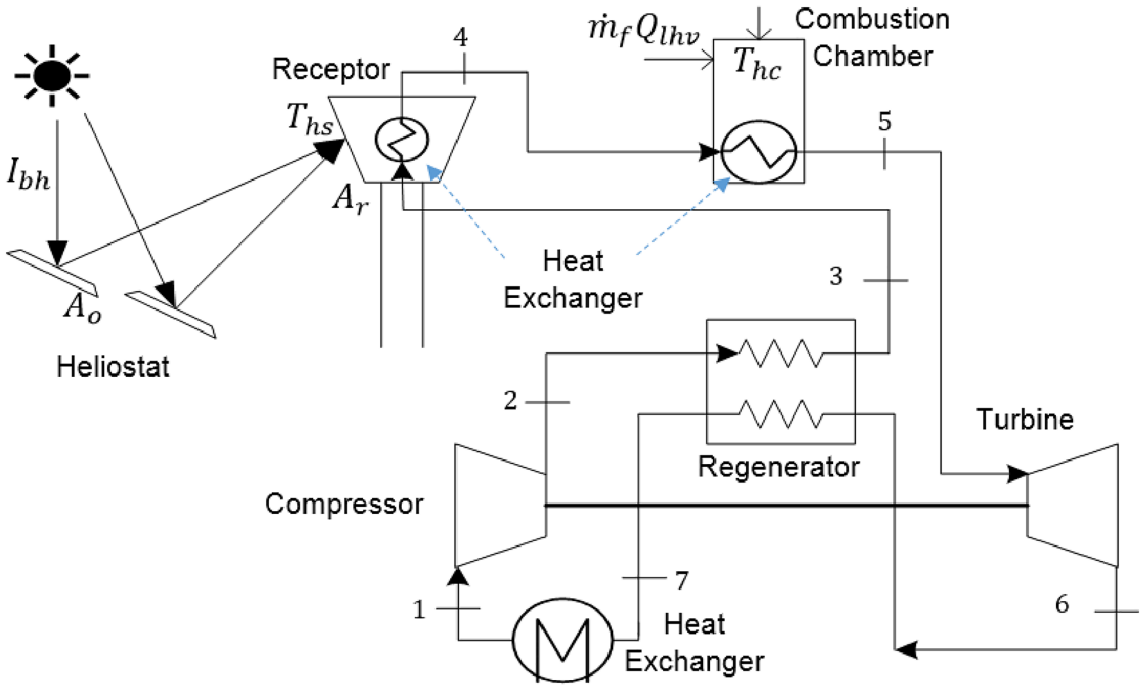

Fig. 2. CSP hybrid power plant scheme.

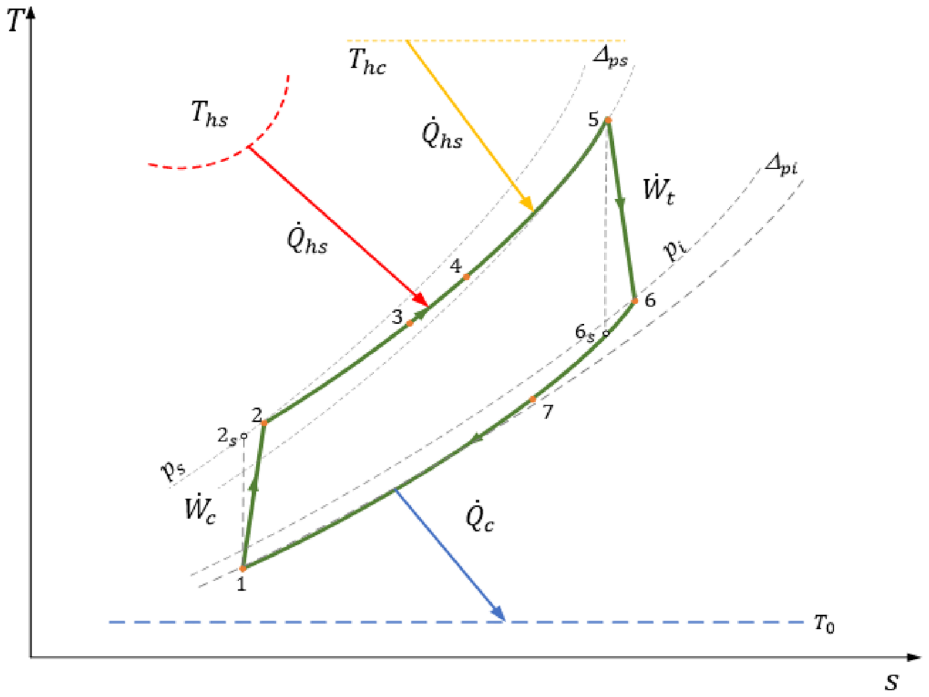

Fig. 3. T-s diagram of the plant.

conditions for both processes are shown in Fig. 3. To include this effect, an overall loss coefficient D_{ps} is defined for the heat supply and D_{pi} for the heat loss [36,35], as

$$D_{ps} = \frac{P_s - \Delta_{ps}}{P_s}, \tag{25}$$

$$D_{pi} = \frac{P_i - \Delta_{pi}}{P_i}, \tag{26}$$

where P_s and P_i are the high- and low- pressure values of the cycle, respectively. If the heat input processes occurred under isobaric conditions, states 2 to 5 would be on the line P_s; likewise, states 6 to 1 would be on the pressure line P_i, if heat is rejected at constant pressure.

The working fluid leaving the compressor passes through three heating processes. The first one occurs in the regenerator as explained before; the second happens in the solar concentration system, in which the heliostats field receives the solar radiation, reflecting $\dot{Q}_r$ to the central tower receiver as,

$$\dot{Q}_r = \eta_0 A_o \frac{I_{bh}}{1000}. \tag{27}$$

The heat loss, $\dot{Q}_p$, affects the available heat $\dot{Q}_{hst}$, as follows,

$$\dot{Q}_{hst} = \dot{Q}_r - \dot{Q}_p. \tag{28}$$

In Eq. 27, η_0 corresponds to the optical efficiency of the heliostat field and depends on aspects such as losses due to cosine efficiency, surface quality and cleaning, tracking system, reflectivity, among others. In this work, the heliostats field overall efficiency reported in the literature was used [64]. On the other hand, the heat loss in the receiver, $\dot{Q}_p$, can be evaluated by assigning linear values of the temperature difference for convection and conduction losses, and nonlinear for radiation losses [65]. In this case, the analysis is performed according to the heat loss in the central receiver expressed as,

$$\dot{Q}_p = A_r \left[h_w (T_{hs} - T_0) + U_{cond} (T_{hs} - T_0) + \alpha\sigma (T_{hs}^4 - T_0^4)\right], \tag{29}$$

where T_{hs} is the temperature of the central receiver, h_w and U_{cond} are the convection and conduction heat transfer coefficients respectively, α is the surface emissivity in the central receiver, σ is Stefan–Boltzmann's constant and A_r is the receiver area. In Eq. 29, a global heat transfer coefficient, U_l, can be included that joins h_w and U_{cond} coefficients; then, $\dot{Q}_p$ is rewritten as,

$$\dot{Q}_p = A_r \left[U_l (T_{hs} - T_0) + \alpha\sigma (T_{hs}^4 - T_0^4)\right]. \tag{30}$$

The receiver transfers heat, $\dot{Q}_{hs}$, to the working fluid (Process 3–4) at the heat exchanger as,

$$\dot{Q}_{hs} = \varepsilon_{is} \dot{Q}_{hst} = \dot{m}(h_4 - h_3), \tag{31}$$

with the effectiveness ε_{is} [33,66], defined as,

$$\varepsilon_{is} = \frac{T_4 - T_3}{T_{hs} - T_3}. \tag{32}$$

The solar concentration system efficiency is defined as,

$$\eta_s = \frac{\dot{Q}_r - \dot{Q}_p}{\frac{I_{bh} A_o}{1000}}. \tag{33}$$

Replacing Eqs. 30 to 32 in Eq. 33, permits to rewrite η_s, as

$$\eta_s = \eta_0 - \frac{U_l (T_{hs} - T_0) - \alpha\sigma (T_{hs}^4 - T_0^4)}{\frac{I_{bh}}{1000} \frac{A_o}{A_r}}. \tag{34}$$

The third and last heat addition to the working fluid (Process 4–5), occurs in the combustion chamber, according to,

$$\dot{Q}_{hct} = \eta_{cc} \mathrm{LHV} \dot{m}_f, \tag{35}$$

being η_{cc} the efficiency of the combustion chamber, LHV the Lower Heating Value of fuel, and $\dot{m}_f$ the fuel mass flow rate. Similar to the receiver, the heat is transferred to the working fluid in the combustion chamber, $\dot{Q}_{hc}$, by using a heat exchanger as,

$$\dot{Q}_{hc} = \varepsilon_{ic} \dot{Q}_{hct} = \dot{m}(h_5 - h_6), \tag{36}$$

where the heat exchanger effectiveness ε_{ic} is defined as [33,66],

$$\varepsilon_{ic} = \frac{T_5 - T_5}{T_{hc} - T_4}. \tag{37}$$

The values of $\dot{Q}_{hs}$ and $\dot{Q}_{hc}$, represent the external heat transfer to the working fluid from the solar concentration system and the combustion chamber, respectively. Thus, $\dot{Q}_h$, the total heat transfer, is defined as:

$$\dot{Q}_h = \dot{Q}_{hs} + \dot{Q}_{hc} = \dot{m}(h_5 - h_3). \tag{38}$$

The solar factor, f, is evaluated at the heat receiver, as:

$$f = \frac{\dot{Q}_{hs}}{\dot{Q}_h} = \frac{\dot{Q}_{hs}}{\dot{Q}_{hc} + \dot{Q}_{hs}}. \tag{39}$$

Additionally, heat is transferred to the surroundings, $\dot{Q}_a$, is expressed as,

$$\dot{Q} = \dot{} (h_7 - h_1), \tag{40}$$

with an effectiveness ε_l, expressed as [33,35],

$$\varepsilon_l = \frac{T_1 - T_7}{T_0 - T_7} \tag{41}$$

The Brayton heat engine efficiency, eta_h, is defined as

$$\eta_h = \frac{\dot{W}_{net}}{\dot{Q}_h}, \tag{42}$$

being the net solar thermal power, $\dot{W}_{net}$, evaluated as,

$$\dot{W}_{net} = \dot{W}_t - \dot{W}_c. \tag{43}$$

The overall plant efficiency can be expressed in terms of the turbine and compressor power, the energy injected by the fuel and direct radiation, as,

$$\eta = \frac{\dot{W}_t - \dot{W}_c}{\dot{m}_f \,\mathrm{LHV} + \frac{I_{bh} A_o}{1000}}. \tag{44}$$

Finally, the fuel conversion rate of the plant is defined as the power generated over the heat released from the fuel [35],

$$r_e = \frac{\dot{W}_{net}}{\dot{m}_f \,\mathrm{LHV}}. \tag{45}$$

Although the fuel conversion rate is not a thermodynamic efficiency, it allows considering the effect of fuel consumption over the plant performance.

2.3. The exergy model of the hybrid thermal solar plant

In this section, exergy balances for each component reduce to a single constant flow system assuming that kinetic and potential exergy changes are neglected, as wells as the chemical exergy at each of the components in the cycles are defined as follows [67,68],

$$\sum_j \dot{E}_{q,j} - \dot{W}_c + \sum_i \dot{m}_i e_i - \sum_e \dot{m}_e e_e - \dot{E}_{d,j} = 0, \tag{46}$$

being $\dot{E}_{q,j}$ the exergy associated with the heat transfer defined as,

$$\dot{E}_{q,j} = \left(1 - \frac{T_0}{T_j}\right)\dot{Q}_j. \tag{47}$$

Additionally, in Eq. 46, $\dot{E}_{d,j}$ corresponds to the destruction of exergy, e_i and e_e are the exergies associated with the mass flow, expressed as

$$e = h - h_0 - T_0(s - s_0), \tag{48}$$

being h and s the enthalpy and specific entropy, respectively. The subscript 0 represents the properties of the working fluid at the environmental conditions. The compressor exergy destruction is evaluated as,

$$\dot{E}_{d,c} = \dot{m}[(h_1 - h_2) - T_0(s_1 - s_2)] + \dot{W}_c, \tag{49}$$

while the same expression for the turbine is,

$$\dot{E}_{d,t} = \dot{m}[(h_5 - h_6) - T_0(s_5 - s_6)] - \dot{W}_t. \tag{50}$$

In the same way, the regenerator exergy destruction is expressed as,

$$\dot{E}_{d,r} = \dot{m}[(h_6 - h_7 + h_2 - h_3) - T_0(s_6 - s_7 + s_2 - s_3)]. \tag{51}$$

Additionally, between states 7 and 1, the CSP plant dissipates heat to the environment at a temperature T_0; with an exergy destruction associated to that process as follows,

$$\dot{E}_{d,a} = \dot{m}[(h_7 - h_1) - T_0(s_7 - s_1)]. \tag{52}$$

For exergy destruction in the combustion chamber, the control volume contains both the combustion chamber and its heat exchanger (see Fig. 4). The general exergy balance at the combustion chamber is expressed as,

$$\dot{E}_{d,cc} = \dot{m}_a E_{m,a} + \dot{m}_f E_{m,f} - (\dot{m}_a + \dot{m}_d) E_{m,g} + \dot{m}[(h_4 - h_5) - T_0(s_4 - s_5)], \tag{53}$$

where $E_{m,a}$, $E_{m,f}$ and $E_{m,g}$ are the specific exergy of the air, the fuel and exhaust gases, respectively. The above specific exergy values are estimated from the mixture relation ratio expressed as $E_m = E_q/PM_m$ [53], being PM_m the molar mass of the mixture and E_q the chemical exergy of natural gas, air or combustion products, which are estimated by,

$$E_q = \sum_{i=1}^{j} y_i E_i + R_g T_0 \sum_{i=1}^{j} y_i \ln y_i, \tag{54}$$

being y_i the fraction and E_i the specific exergy of each component in the fuel, and R_g the universal constant of gases. Therefore, it is possible to determine the exhaust gases, the fuel and air inflow exergy destruction for each stream to and from the combustion chamber.

Regarding the solar concentration system, the solar exergy total input to the system is defined from the maximum available useful work as a function of radiation according to [69,70],

$$\dot{E}_{x,s} = \frac{I_{bh}}{1000} A_o \left[1 + \frac{1}{3}\left(\frac{T_0}{T_s}\right)^4 - \frac{4}{3}\frac{T_0}{T_s}\right], \tag{55}$$

while the total exergy at the receiver from the heliostat field is,

$$\dot{E}_{x,i} = \dot{Q}_r\left(1 - \frac{T_0}{T_{hs}}\right). \tag{56}$$

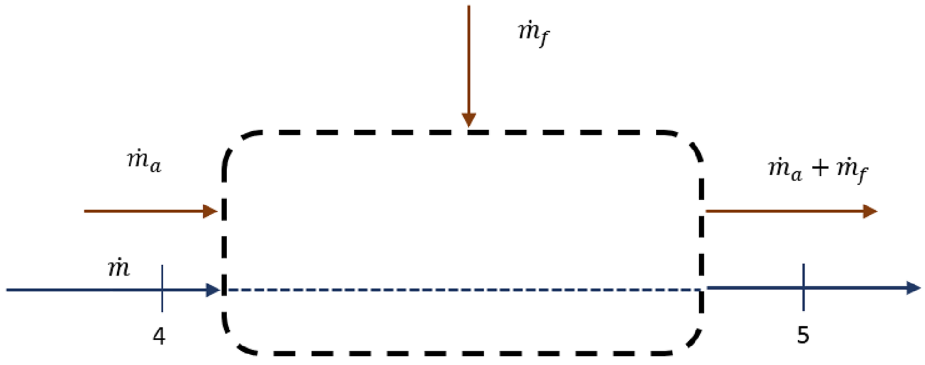

Fig. 4. Control volume for the combustion chamber and its heat exchange.

Therefore, the exergy destroyed by the field of heliostat is,

$$\dot{E}_{d,he} = \dot{E}_{x,s} - \dot{E}_{x,i}. \tag{57}$$

For the solar receiver, the destruction of exergy is,

$$\dot{E}_{d,rc} = \dot{Q}_{hs}\left(1 - \frac{T_0}{T_{hs}}\right) + \dot{m}\left[(h_3 - h_4) - T_0(s_3 - s_4)\right]. \tag{58}$$

The total exergy destroyed by the solar thermal plant $\dot{E}_{d,T}$, is defined as

$$\dot{E}_{d,T} = \dot{E}_{d,c} + \dot{E}_{d,t} + \dot{E}_{d,a} + \dot{E}_{d,cc} + \dot{E}_{d,he} + \dot{E}_{d,rc}, \tag{59}$$

while the overall exergetic efficiency η_{ex} can be expressed in the following way,

$$\eta_{ex} = \frac{\dot{W}_{net}}{\dot{E}_{x,s} + \dot{m}_f E_{m,f}}, \tag{60}$$

and the exergetic efficiency of the Brayton heat engine eta_{exh},

$$\eta_{exh} = \frac{\dot{W}_{net}}{\dot{m}\left[(h_3 - h_4) - T_0(s_3 - s_4)\right]}. \tag{61}$$

Finally, the fraction of exergy destruction in each component is evaluated as,

$$FE_{d,j} = \frac{\dot{E}_{d,j}}{\dot{E}_{d,T}}. \tag{62}$$

3. Validation of the solar model and site selection

The solar resource model assessment with data reported by peers is presented in this section. Available solar resource of three Colombian cities is analysed regarding monthly values of global, $\overline{H}_h$, and diffuse, $\overline{D}_h$h, solar radiation to establish the most suitable place to simulate a hybrid solar plant under specific radiation conditions of the selected city.

3.1. DNI model validation

The daily integration model, presented in Section 2.1 (see Eq. 4), is used in this work to evaluate the hourly DNI for three Colombian cities. The DNI model is assessed with solar radiation data reported for Sevilla (San Lucar meteorologic station); to evaluate the direct radiation of the Colombian sites. Regarding the Sevilla case, the global radiation value for the day selected is 7.8 kWh/m^2/day with corresponding diffuse radiation of 1.7 kWh/m^2/day [63]. The latitude of the place is 37.38° north. Data are taken for day $n = 210$, corresponding to July 20. Fig. 5 presents San Lucar meteorologic station measurement of direct radiation, $I_{bh,m}$, (blue triangles) and results from the DNI model evaluation, $I_{bh,c}$, (red circles) through the indicated day [71].

Following the methodology proposed in [60,61,63], the values obtained with the DNI model and those reported by the San Lucar station are compared by evaluating the Mean Absolute Bias Error (MABE) and the Root Mean Square Error (RMSE). The MABE provides long-term performance information of the correlation allowing a comparison of the actual deviation between calculated and measured values, term by term through the absolute value of their difference as follows,

$$\text{MABE} = \frac{1}{N_d}\sum_{i=1}^{N_d}\left[|I_{bh,e} - I_{bh,m}|\right]. \tag{63}$$

Conversely, the Root Mean Square Error (RMSE) provides information in the short term and is determined as,

$$\text{RMSE} = \sqrt{\frac{1}{N_d}\sum_{i=1}^{N_d}(I_{bh,e} - I_{bh,m})^2}. \tag{64}$$

For instance, the MABE of the data obtained with the DNI model is 0.201, which is the range of 0 to 0.212 reported by Yao et al. [61]. Also, the RMSE attains a value of 0.227 within the scope of 0 to 0.329 related in [60,61]. The DNI model implemented achieves results fitted in good agreement with the experimental data, as observed in Fig. 5 with an acceptable error level. Then, in the following sections, the DNI model stated in Eq. 4 will be used to evaluate the hourly direct radiation of the cities with the potential to implement CSP plants in Colombia.

3.2. Selection of a Colombian city for the simulation of the hybrid thermal solar plant under specific conditions

Fig. 6 shows the monthly average daily data through the year of

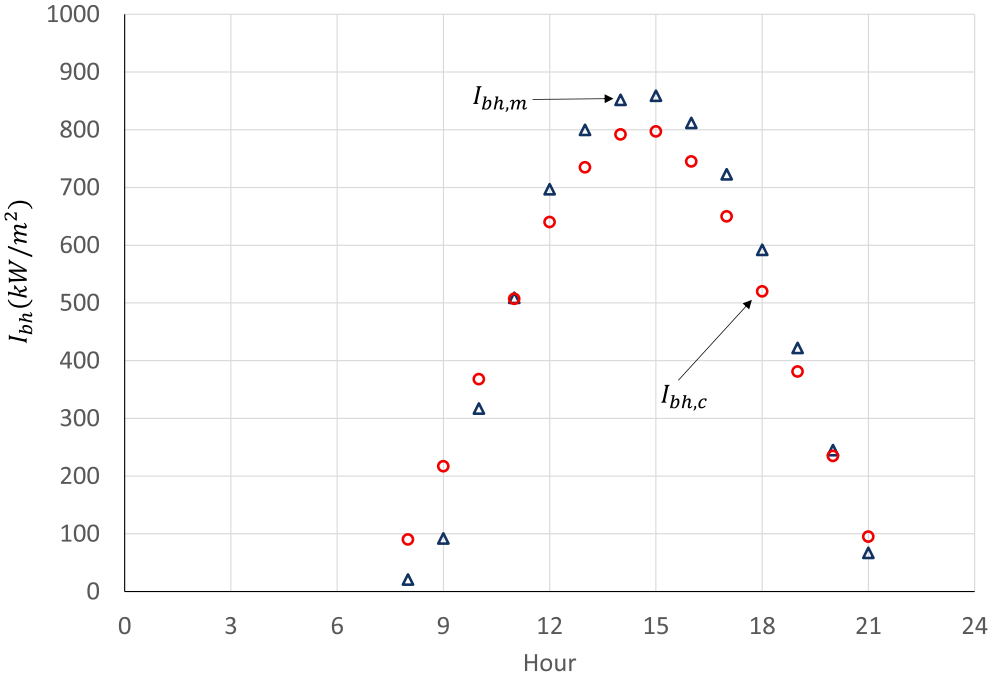

Fig. 5. Estimated $I_{bh,e}$ and measured $I_{bh,m}$ direct solar radiation for Seville.

global radiation for three Colombian cities: Cúcuta, Cartagena, and Barranquilla. These cities were chosen due to the proximity to conventional thermal power plants, availability of natural gas and their demographic expansion. Regarding the solar resource, as can be observed in Fig. 6, the global radiation has a slight variation throughout the year for all three Colombian cities, with the following lower and upper limits: Cúcuta 4.47 and 5.09 kWh/m^2/day; Cartagena 4.45 and 6.46 kWh/m^2/day and Barranquilla 5.44 and 6.99 kWh/m^2/day. Fig. 6 also shows values for the monthly average daily data through the year of global radiation for Seville (Spain). The lower and upper limits for that city are 2.17 and 7.8 kWh/m^2/day, respectively, implying a higher variation during the year (as can be observed from the figure).

Fig. 7 shows the evolution of diffuse radiation throughout the year. The central receptor heat rate input (and then, the plant output power) is directly proportional to the difference between the global and direct radiation (see Eq. 27). From the values above, it is possible to confirm that Cúcuta has the lowest variation throughout the year for both global and diffuse radiations. Meanwhile, Barranquilla presents the most moderate values of diffuse radiation compared to the other cities (1.09 and 2.04 kWh/m^2/day), and are even closer to those reported in the case of Seville (0.76 and 2.04 kWh/m^2/day). Fig. 7,8 presents the average annual values of $\overline{H}_h$ and $\overline{D}_h$ for the three Colombian cities and Seville. It is observed that the highest average annual global radiation values (as well as the monthly average, see Fig. 7) correspond to Barranquilla, even higher than that for Sevilla. Meanwhile, Cúcuta has the lowest value of all three cities.

The behaviour exposed above, together with the thoughtful difference of the global variation throughout the year and the smallest average variation of the diffuse radiation, even compared with Seville, allows us to conclude that from the solar resource point of view, Barranquilla is a good option for evaluating future development of a hybrid solar plant in Colombia. Then, Barranquilla is selected due to the availability of the solar resource, showing a minor resource variation through the year with higher values of global radiation little offset by low amounts of direct radiation. Likewise, the city is close to the power grid with the presence of conventional thermal power plants (as an option to a future diversification of the Colombian energy mix), and availability of fossil fuel sources (natural gas in this case). Additionally, Barranquilla is a significant urban and industrial centre in the region although, it has a very poor power quality and reliability.

The DNI model results for Barranquilla are used to simulate the CSP plant under the specific environmental conditions of this city. In this case, the average annual value of $\overline{H}_h$ is 6.24 kWh/m^2/day and of $\overline{D}_h$ is 1.68 kWh/m^2/day for the day 180 of the year [63]. Fig. 9 shows the results of the I_{bh} for the average annual values (black squares) and when $\overline{H}_h$ is maximum in Barranquilla (blue triangles), that occurs at the middle of March. In the same figure, is also plotted the I_{bh} when $\overline{H}_h$ is maximum for the case of Servile during July (red circles). It can be seen that during the months of the maximum global radiation, the difference of the I_{bh} between Servile and Barranquilla is only 4.8%; however, Seville has more hours of radiation per day as an effect of the seasonality through the year. Fig. 9 also presents average hourly temperature, T_0, for Barranquilla (green dashed line) [72], that will be used to assess the plant performance analysis in the following sections.

4. Energy analysis of a hybrid solar plant

This section presents the performance evaluation of a hybrid solar plant under several conditions. Results reported for the Solugas experimental facility located in Sanlúcar (Seville, Spain) [73], are used to validate the thermodynamic model presented in Section 2.2. Section 4.1 offers the energy performance of the plant in terms of the evolution of temperatures and derivated variables at different states through the cycle. Power plant output and thermal efficiency behaviours are also studied, as well as the influence of the pressure ratio and local radiation on the plant operation are presented in Section 4.2 for specific conditions of the city selected in Section 3.2.

4.1. Validation of the thermodynamic model for the hybrid thermosolar plant

The thermodynamic model validation is carried out with information from the Solugas experimental plant, a research project by the Abengoa Company in the vicinity of Seville (Spain). That pilot plant has a central tower system of 75 m high and a field of 69 heliostats, each of them with a 121 m^2 reflective area [73]. The thermal plant has a

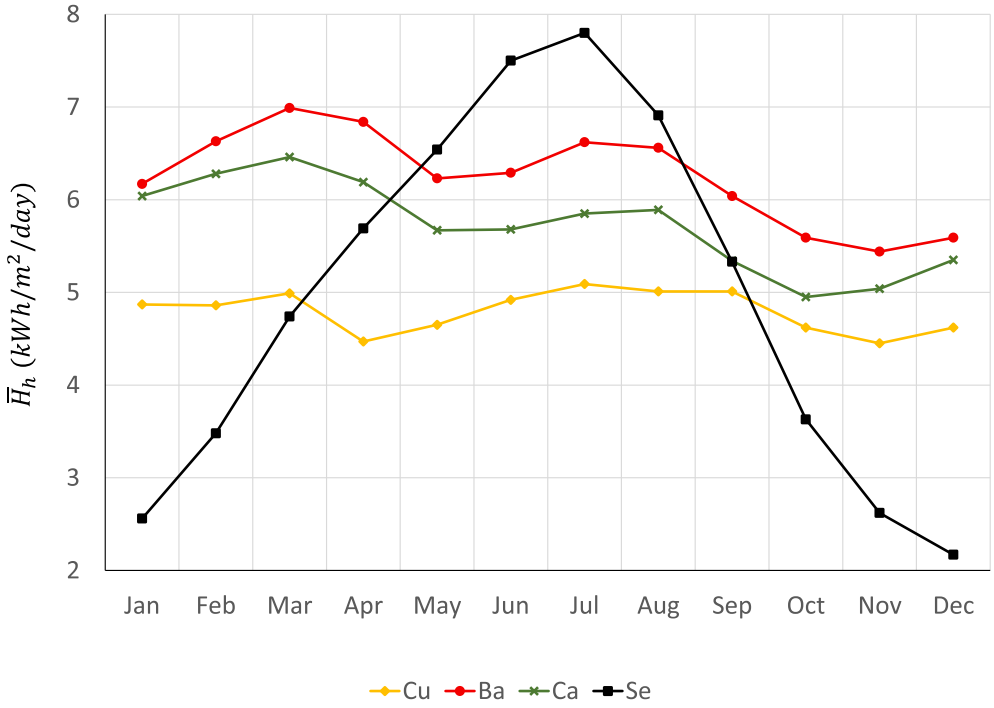

Fig. 6. Global radiation through the year for Cúcuta (CU), Barranquilla (BA), Cartagena (CA) and Seville (SE).

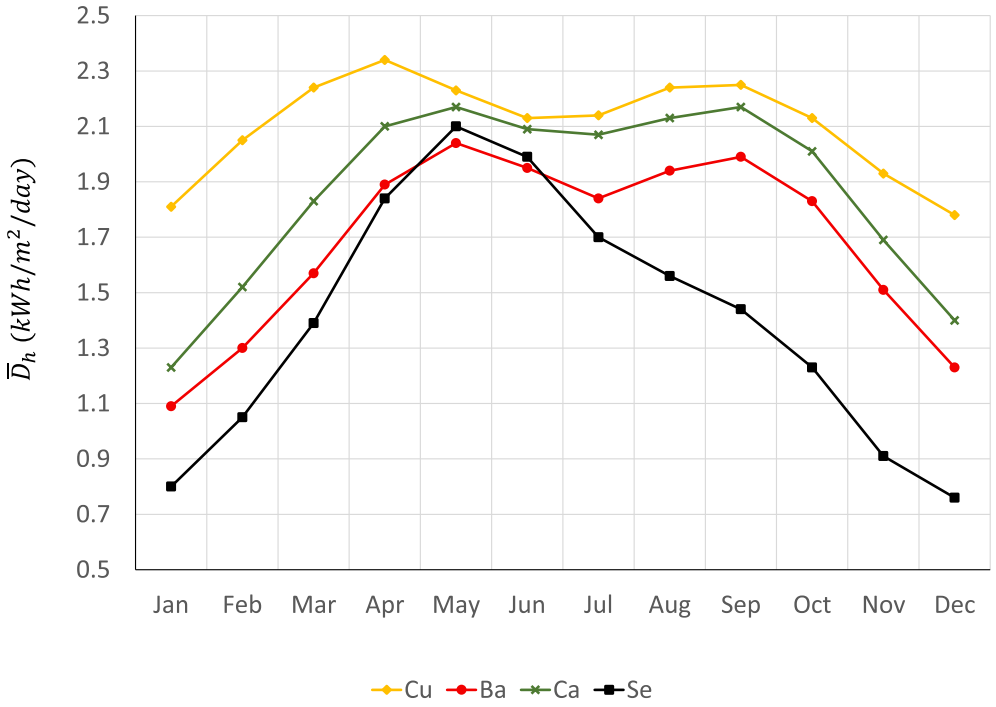

Fig. 7. Diffuse radiation through the year for Cúcuta (CU), Barranquilla (BA), Cartagena (CA) and Seville (SE).

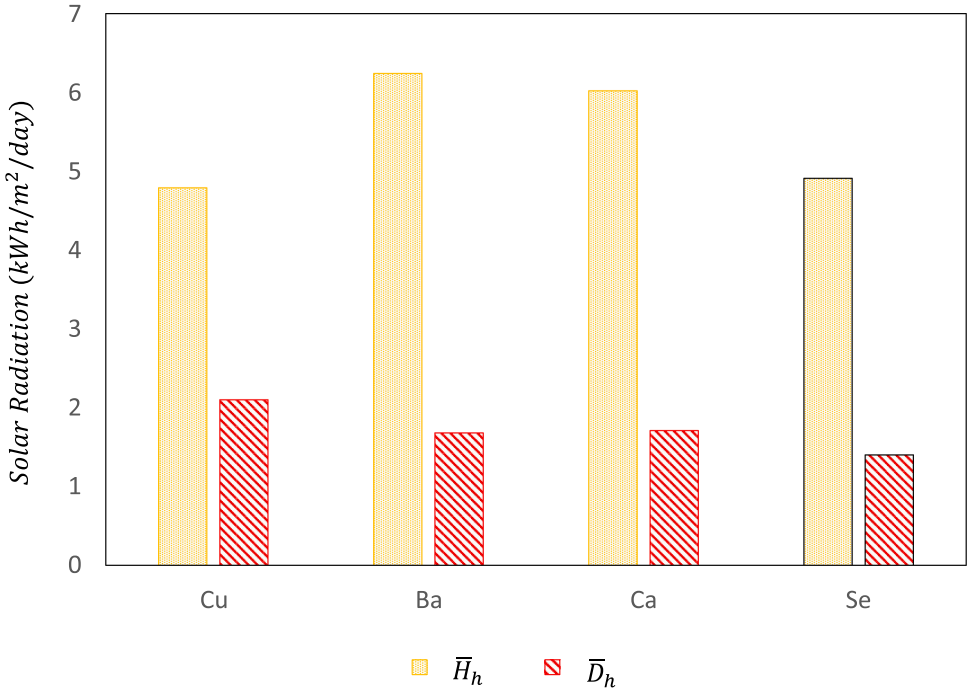

Fig. 8. Annual average values for $\overline{H}_h$ and $\overline{D}_h$ for Cúcuta (CU), Barranquilla (BA), Cartagena (CA) and Seville (SE).

Table 1
Thermodynamic model assessment with data from the turbine manufacturer working at full load on only combustion mode.

	$\dot{W}_{net}$ [kW]	η_h	T_5 [K]
Model	4635.4	0.385	1422
Reference [74]	4600	0.39	1423
Error %	0.7	1	0.07

Table 2
Thermodynamic model assessment with data reported of the Solugas plant.

	T_2 [K]	T_5 [K]	T_7 [K]
Model	620	1422	914
Reference [73]	603	1423	921
Error %	2.8	0.07	0.7

Table 3
Thermodynamic model assessment with data from [35].

	η	f	T_4 [K]	$\dot{m}_f$ [kg/s]
Model	0.298	0.327	1042.9	0.176
Reference [35]	0.300	0.341	1027	0.172
Error %	0.66	4.1	1.5	2.3

Caterpillar Mercury 50 gas turbine [74]. The Solugas plant is the first hybrid thermosolar plant with a Brayton cycle in the scale of MW, therefore complete and detailed results are unknown. However, the general description of the operation and configuration reported allows to simulate its performance [33]. The solar concentration system has an emissivity $\alpha = 0.1$, an overall heat loss coefficient $U_L = 5\ \mathrm{Wm^{-2}K^{-1}}$, and an optical efficiency $\eta_o = 0.73$ [38,75] [15,58]. The solar field concentration relationship is $C = A_o/A_r = 425.2$, the heliostats area field is $A_o = 8349\ \mathrm{m^2}$ and the receiver area is $A_r = 19.63\ \mathrm{m^2}$.

The Caterpillar Mercury 50 gas turbine has a pressure ratio $r_p = 9.9$, operates with an air mass flow rate $\dot{m}_f = 17.9$ kg/s, a combustion chamber operating temperature of $T_{hc} = 1430$ K, and operates at an ambient temperature $T_0 = 288$ K [74]. Also, the regenerator effectiveness is $\varepsilon_r = 0.775$. Regarding global pressure losses during the heat absorbing and dissipating process, pressure loss coefficients $D_{ps} = D_{pi} = 0.908$ are defined, representing approximately 9.2% of relative pressure loss in each of them [36,35,76]. Likewise, the effectiveness of the heat exchanger associated with the receiver, the combustion chamber and for heat dissipated to the environment are defined as $\varepsilon_{hs} = 0.8$, $\varepsilon_{hc} = 0.98$ and $\varepsilon_l = 1.00$, respectively. The latter implies that all the heat available in the working fluid is delivered to the environment as if the cycle was open. In the same way, the isentropic efficiencies of the compressor and the turbine are $\eta_c = 0.815$ and $\eta_t = 0.885$ [33,35]. The compressor inlet pressure is settled to $P_1 = 111.5$ kPa.

Initially, the thermodynamic model is assessed with data reported by the turbine manufacturer comparing the power output, $\dot{W}_{net}$, the heat engine efficiency, η_h and the turbine inlet temperature, T_5 (see Table 1). The model implemented in Dymola ® for this work is capable of reproducing the power output with a deviation below 0.7% and the heat engine efficiency below 1%. Table 2 presents results for temperature values at the compressor outlet T_2 and turbine inlet T_5 and outlet T_6, and the corresponding data reported for the Solugas plant [73], where minimal variations are observed. Finally, the overall plant efficiency, η, the solar fraction, f, and fuel consumption, $\dot{m}_f$, are compared with results reported in [35], where an excellent adjustment of the model is obtained. The results in Table 3 show that the highest error (i.e., 4.1%) is gathered for the solar factor while the other components and variables are kept below 2.3%. For the validation, the direct radiation used was $I_{bh} = 860\ \mathrm{W/m^2}$ and a lower heating value for the natural gas of LHV = 47121 kJ/kg [35]. These results allow checking the capacity of the model applied for the study of CSP plants under different conditions.

4.2. Energy performance analysis for the solar plant under Colombian conditions

This section presents the energy evaluation of the solar plant under the Barranquilla conditions, as indicated in Section 3.2. The objective of this section concerns the performance evaluation of the CSP under the specific site and operating conditions. It includes the influence of (1) ambient and turbine inlet temperature; (2) the system pressure ratio; and, (3) available radiation in Barranquilla considering the month with highest and lowest monthly global average daily radiation. For all simulations, the lower heating value of the fuel is set to LHV = 42624 kJ/kg according to the natural gas available in the area.

4.2.1. Ambient and turbine inlet temperature effect over CSP performance

Gas turbine performance is affected by anything that changes the density and mass flow rate of the air intake to the compressor, being ambient temperature one of the main variables that have a significant impact on working fluid's temperature. It has been estimated that an increase in this parameter conduces to a decrease in the turbine power output affecting the overall thermal plant efficiency. In this regard, Barigozzi [77] estimates that for a 10 °C rise in the ambient temperature, power output can decrease between 5% and 13%. The effectiveness of the heat exchanger used to release residual heat from the system

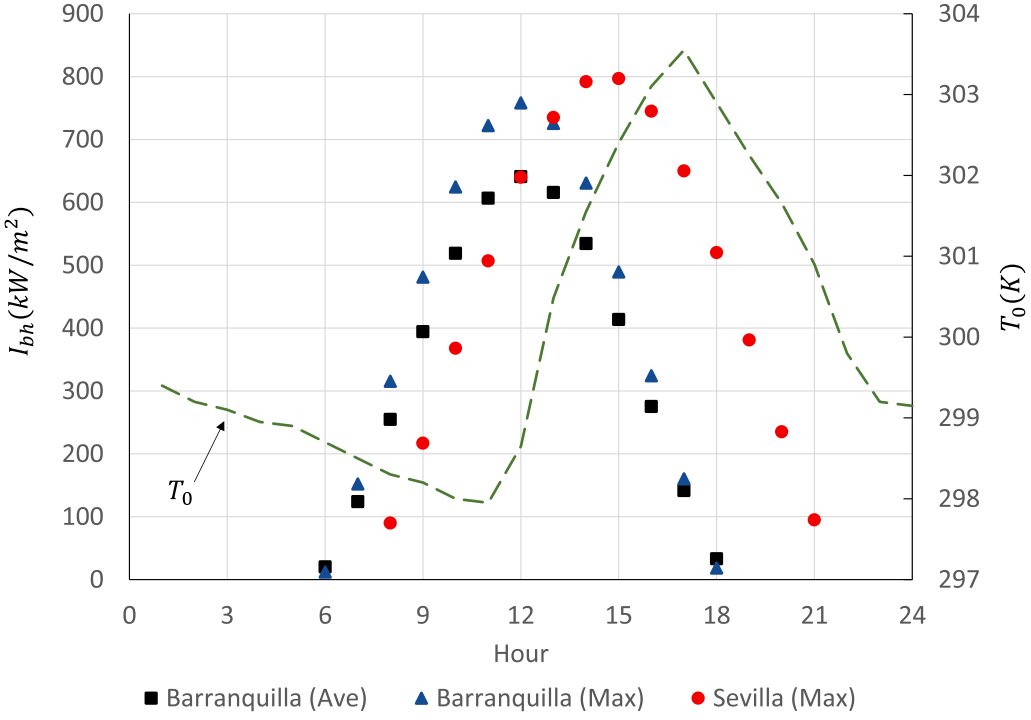

Fig. 9. Comparison of I_{bh} for Seville and Barranquilla.

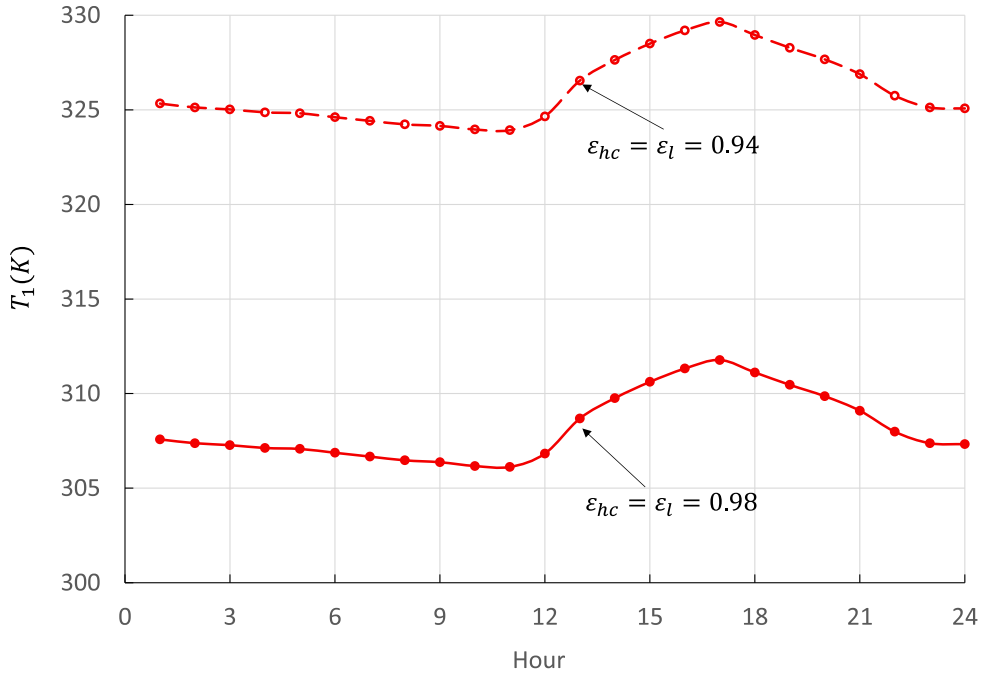

(a)

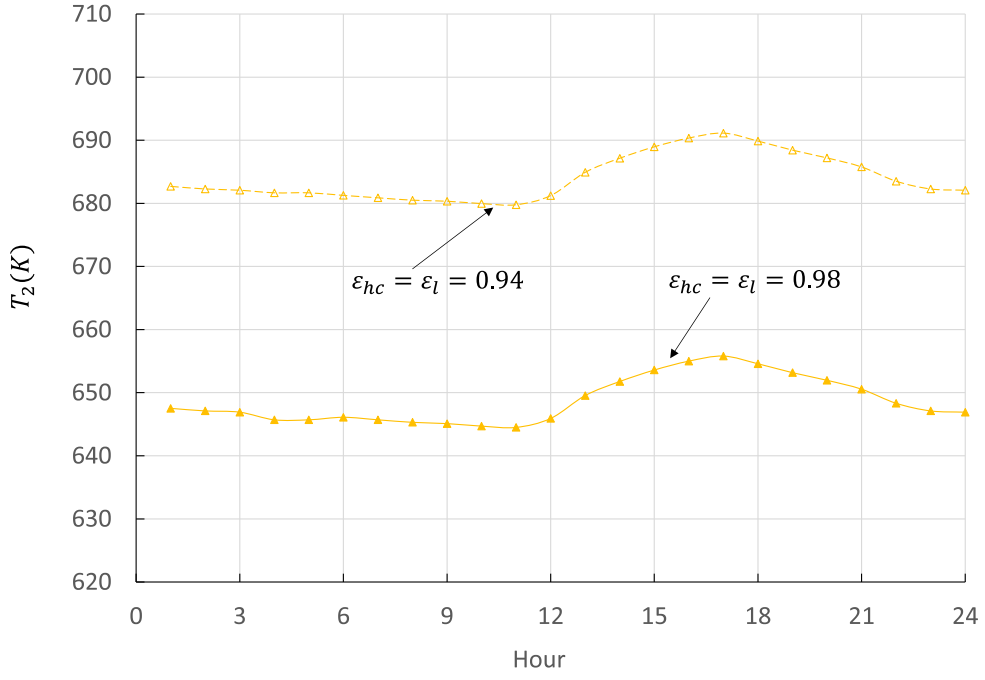

(b)

Fig. 10. Hourly compressor (a) inlet and (b) outlet temperatures.

to its surroundings (process 7–1, Fig. 2) is changed to include the ambient temperature effect on the closed Brayton cycle performance defined in Section 2.2. The effectiveness of the heat exchanger associated with the combustion chamber is also modified (process 5–6, Fig. 2)) to account for the turbine's inlet temperature over the heat engine performance. Heat exchangers' effectiveness can range between 0.8 and 0.94 [78]. Taking into account the previous and considering Solugas plant studies[73], in this work, the effectiveness of both heat exchangers are settled at 0.94 and 0.98. The effect of both effectivenesses on the cycle temperatures are plotted in Figs. 10 to 11.

Fig. 10a shows hourly compressor inlet temperature as a function of heat exchanger effectiveness. For the case when both heat exchanger

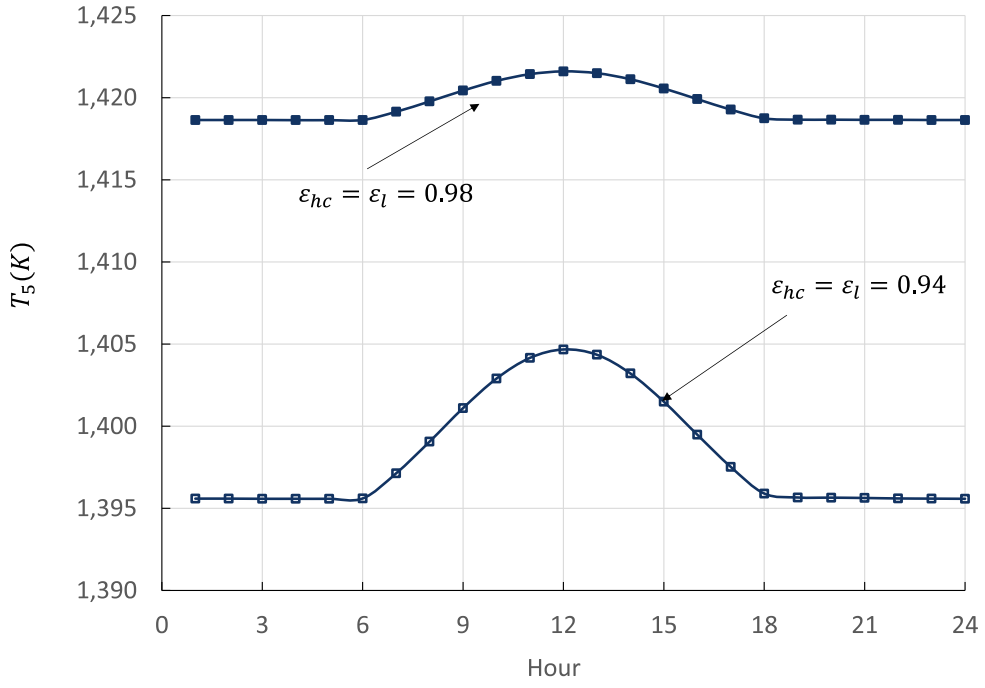

(a)

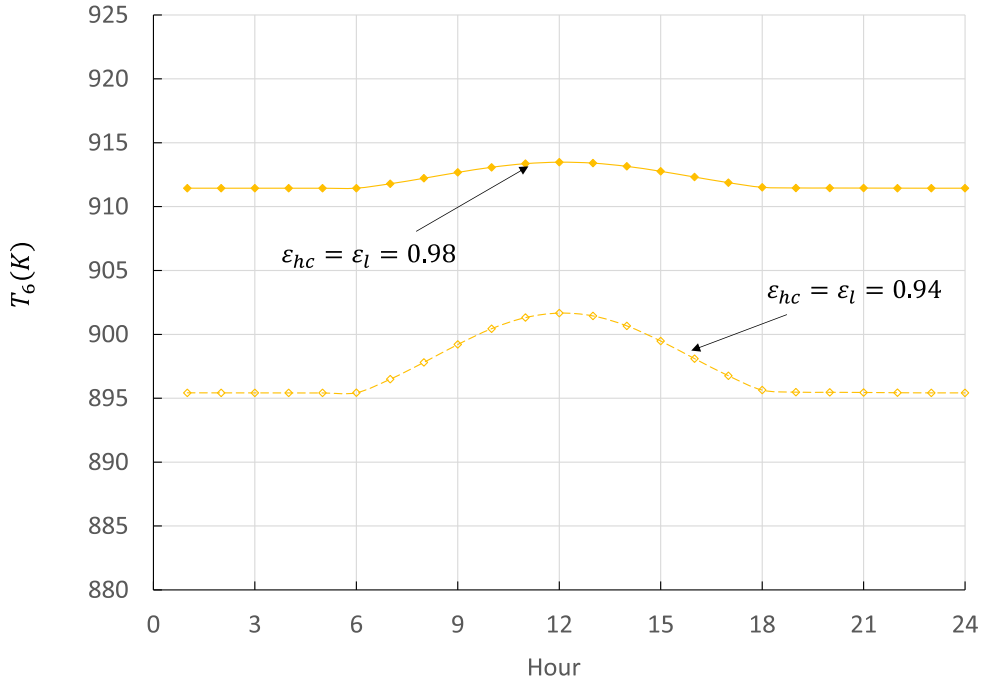

(b)

Fig. 11. Hourly turbine (a) inlet and (b) outlet temperatures.

has an effectiveness of 0.98, the average compressor's inlet temperature is 308 K. As the heat exchanger effectiveness is reduced to 0.94, the average compressor's inlet temperature rises to 325 K, representing a 5.4% increase respect to the previous case. Meanwhile, the average increase in compressor outlet temperature is 5.1% (see Fig. 9,10b). Additionally, the ambient temperature throughout the day (see Fig. 9) influences both temperatures profiles. About the turbine, the inlet temperature presents an average decrease of 1.5% when the heat exchanger effectiveness is reduced from 0.98 to 0.94 as plotted in Fig. 11a; whereas, the outlet temperature diminish 1.7% (see Fig. 11b).

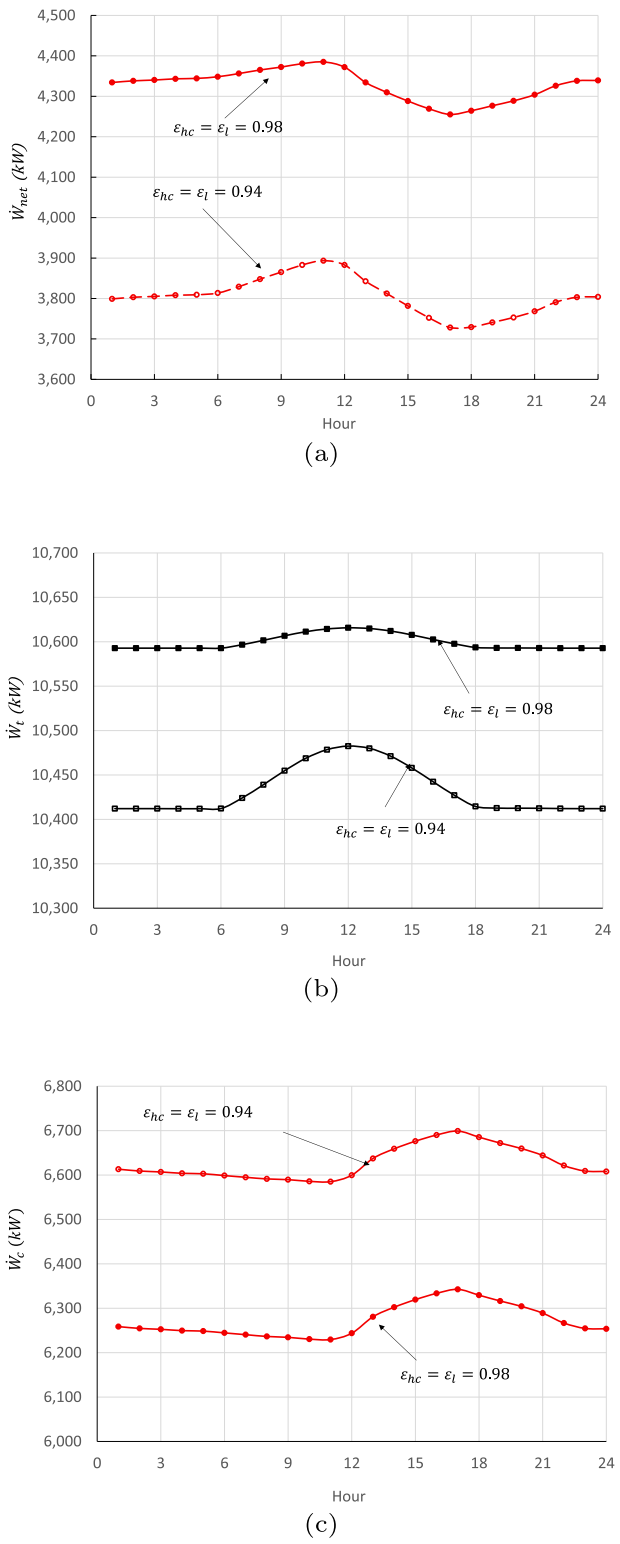

Fig. 12. Daily evolution of net power plant output (a), turbine power outlet (b) and compressor inlet (c) under Barranquilla conditions.

Contrary to the compressor's temperatures trend, the ambient temperature has a minimum effect on inlet and outlet turbine temperatures, being more dominant by the incoming direct radiation and the combustion process.

As expected, the ambient temperature and then compressor and turbine temperatures have a strong influence on the power delivered by the plant, as seen in Fig. 12a, where hourly net power output is plotted. It is possible to observe that a small reduction in heat exchangers' effectiveness (and their corresponding effects on the temperatures) conduce to a significant decrease in the power obtained from the CSP. The decline in net power output is analysed concerning the reference case. Mainly when operating conditions are settled for the reference case and the ambient temperature is changed from 288 K to 298 K, it leads to a reduction in power of 5.1%. Moreover, in this case, when the effectiveness is 0.98 the average power decreases by 6.22%, however, when it is settled to 0.94 the power decreases by 17.5%, compared to the Solugas plant operating conditions. Following [14], to have a quantitative idea of the amplitude of the oscillations due to ambient temperature variations, we have computed the relative amplitude defined as $(P_{max} - P_{min})/P_{min}$, presenting a value of 3.0% when the effectiveness is 0.98 and is 4.5% when the effectiveness is reduced to 0.94.

Fig. 12b shows the turbine outlet power, while Fig. 12c presents the compressor inlet power. As expected, turbine power output increases as the inlet temperature augments; meanwhile, compressor inlet power tends to reduce as the inlet temperature is diminished. The average compressor power inlet is 6626.72 kW when $\varepsilon_{hc} = \varepsilon_l = 0.94$; though, as heat exchangers' effectiveness is increased, the required compressor power reduces to 6271.48 kW, corresponding to 5.3% less power. Meanwhile, the average turbine outlet power only increases by 1.5% with the effectiveness variation, confirming that the compressor inlet temperature is the most critical factor influencing the net power output.

Additionally, since the above results were achieved keeping working fluid mass flow rate constant, any rise in the inlet compressor temperature will result in an expected increase in the compressor inlet power and the subsequent reduction in overall power plant output and efficiency. As observed, in the case of the compressor's temperatures, ambient temperature variation also affects the power required by the compressor and then the released power of the thermal plant throughout the day. Regarding fuel consumption, it maintains a similar behaviour for both heat exchangers' effectiveness, with only 0.7% deviation when there is no solar contribution and 0.3% when it reaches the highest point.

Fig. 13 presents the overall hourly efficiency of the plant, η, and the Brayton heat engine, η_h. It is possible to corroborate that during night hours, the Brayton heat engine and the combustion process mainly dominates the overall efficiency as heat losses affect it to a lesser degree. However, as the solar contribution begins to be significant, the value of η_h decreases (see Fig. 13), mainly due to the increase in solar concentration system losses (i.e., the greater the radiation, the higher the temperature in the concentrator and the greater are the losses). Besides, the efficiency variation is function of the ambient temperature mostly for the heat engine, due to the effect over the compressor behaviour throughout the day.

Overall efficiency is also affected by heat exchangers' effectiveness as well as by the combustion process [33,36]. In this sense, when both heat exchangers' effectiveness are 0.98, the overall plant efficiency presents a maximum of 35.48% and a minimum of 30.01% representing a relative breadth of 18.22%. A reduction in heat exchangers' effectiveness to 0.94 implies that η presents a maximum value of 30.90% and a minimum of 26.56%, which is a relative amplitude of 16.3% (see Fig. 13), having a firm downward on η. On the other hand, hourly Brayton heat engine efficiency is not influenced by the total heat delivered, $\dot{Q}_h$, which is regulated by the heat exchanger associated with the combustion chamber. In this case, the relative amplitude is only 2.2% when $\varepsilon_{hc} = \varepsilon_l = 0.98$. However, the average reduction in η_{hc} is 9% as the heat exchanger effectiveness is reduced (see Fig. 13).

Regarding the efficiency of the solar receiving subsystem, η_s, neither the variation in the ambient temperature nor the heat exchanger's effectiveness has a significant effect on it, representing a changing in this value that not exceed 0.02%. This behaviour is because η_s only depends on the solar resources and the concentration system. Solar efficiency is only evaluated when the solar resource contributes to the plant

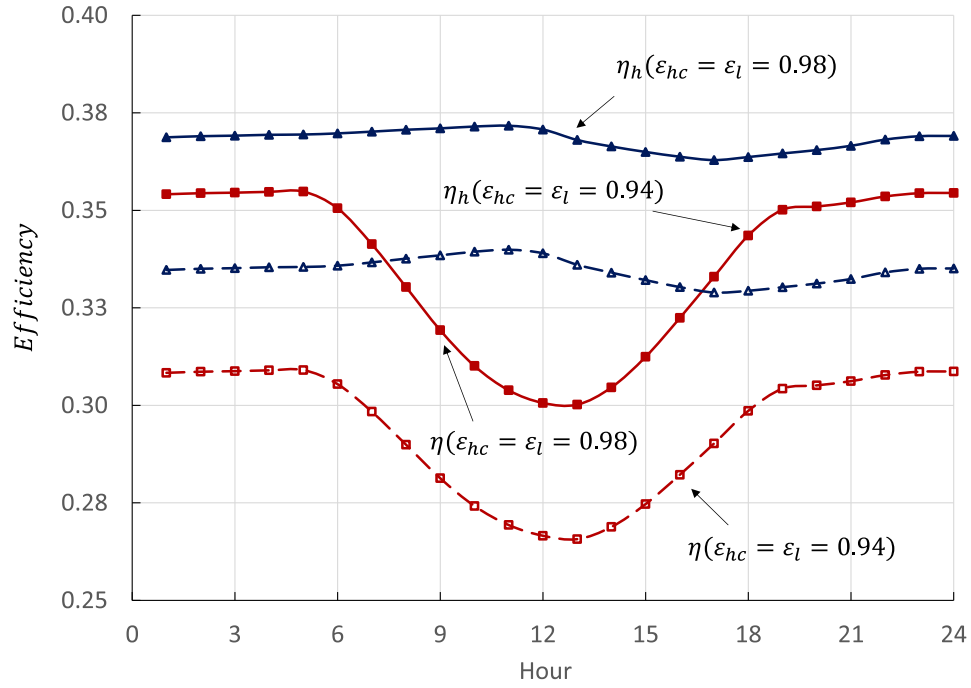

Fig. 13. Daily evolution of overall plant efficiency, η, and Brayton heat engine efficiency, η_h.

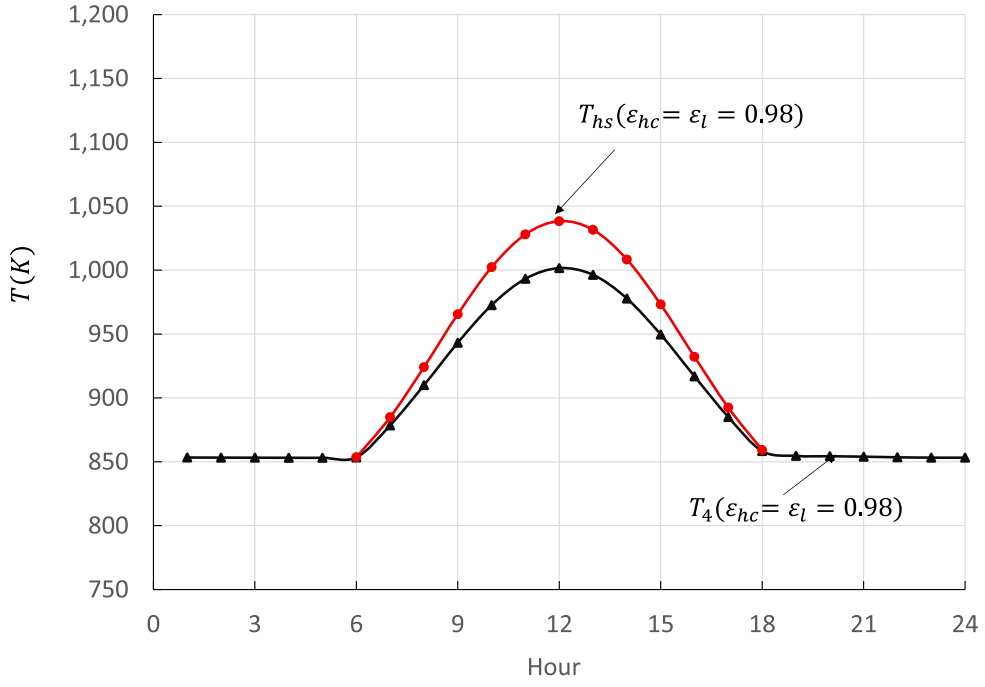

Fig. 14. Hourly central receiver temperature T_{hs} and receiver outlet working fluid temperature T_4.

operation (i.e., when the concentration system provides effective heat to the working fluid). It presents a minimal variation throughout the day; increasing during the first hours of the morning and a decreasing at the end of the afternoon. The above behaviour is explained because any increase in the solar resource conduce to a rise in the receiver temperature, T_{hs}, and therefore in the heat losses to the ambient. The behaviour of η_s through the day is a function of the solar radiation showing not much variation in regions near the equatorial line throughout the year. It is crucial to indicate that reference values were used for the development of the present work and a constant amount of η_0 was used and no transient behaviour of T_{hs} as function of I_{bh} was reported in [35].

Finally, temperatures influenced by the solar concentration system are shown in Fig. 14–16. The receiver outlet working fluid temperature, T_4, presents a difference that does not exceed 1% for both of the heat exchanger's effectiveness. Additionally, it is essential to observe that T_4 has a parabolic shape that matches the pick of the solar resource and keeps below the solar receiver temperature, T_{hs}. This temperature reaches its maximum point around noon when heat losses in the receiver are higher and T_{hs} is 3.53% greater than T_4.

4.2.2. *Influence of the pressure ratio on CSP plant performance*

The pressure ratio has a significant effect on gas turbine performance. In this section, the influence of this variable is analysed

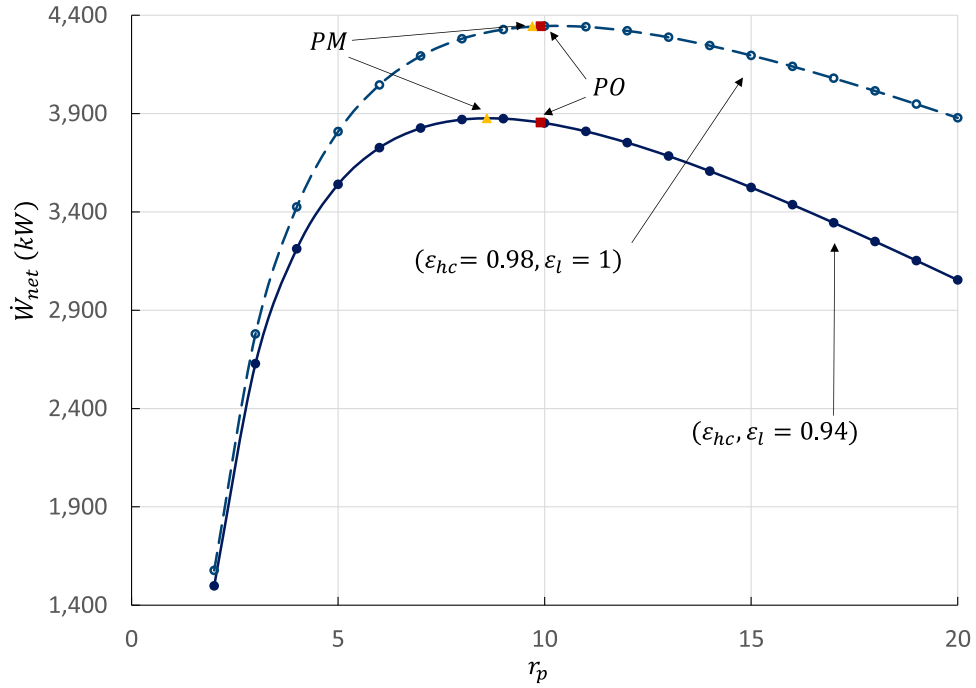

Fig. 15. Influence of the pressure ratio on the power generation.

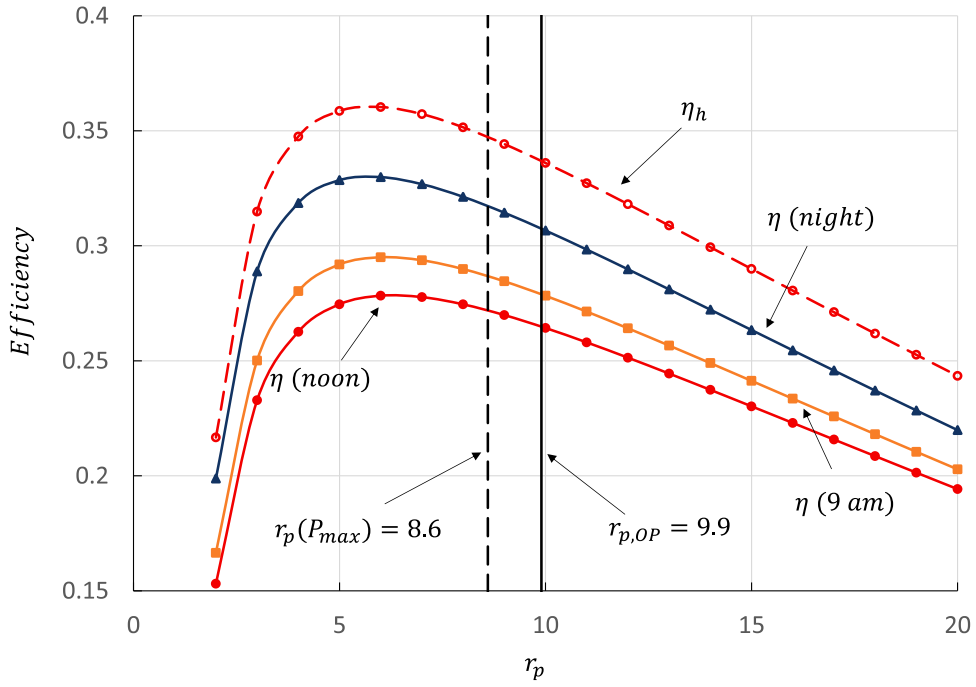

Fig. 16. Influence of the pressure ratio on the overall and heat engine efficiency at different moment during the day.

Table 4
Optimum points of efficiency.

	η (night)	η (9 A.M.)	η (noon)	η_h
r_p	6	6.1	6.4	6.8
Value	0.3298	0.2950	0.2756	0.3604

concerning the efficiency and power output behaviour. Simulations were developed with an average constant ambient temperature of 300 K and varying CSP plant pressure ratio, r_p, between 2 and 20. The heat exchanger effectiveness associated with the combustion chamber and the one used to release residual heat from the system to its surroundings is modified. First, net power output is assessed considering values for $\varepsilon_{hc} = 0.98$ and $\varepsilon_l = 1$, corresponding to values currently used for the thermodynamic model validation and operation condition of the Solugas plant (Section 4.1). The second case corresponds to the specifications when $\varepsilon_{hc} = \varepsilon_l = 0.94$, as reported in Section 4.2.

Fig. 15 shows results for both cases considering the influence of the pressure ratio on the net power output. The first case (dashed line) corresponds to the operation of an open cycle (i.e., $\varepsilon_l = 1$ means all the heat available in the working fluid is delivered to the environment). As can be observed, the maximum power (MP) is obtained for $r_p = 9.7$,

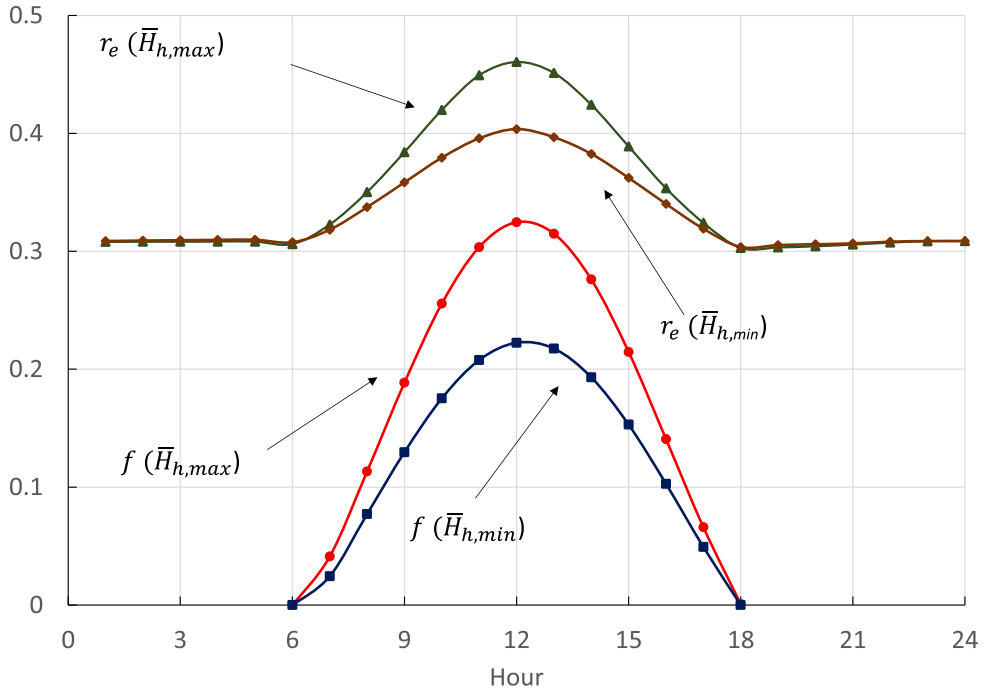

Fig. 17. Daily evolution of global radiation on solar share and fuel conversion rate.

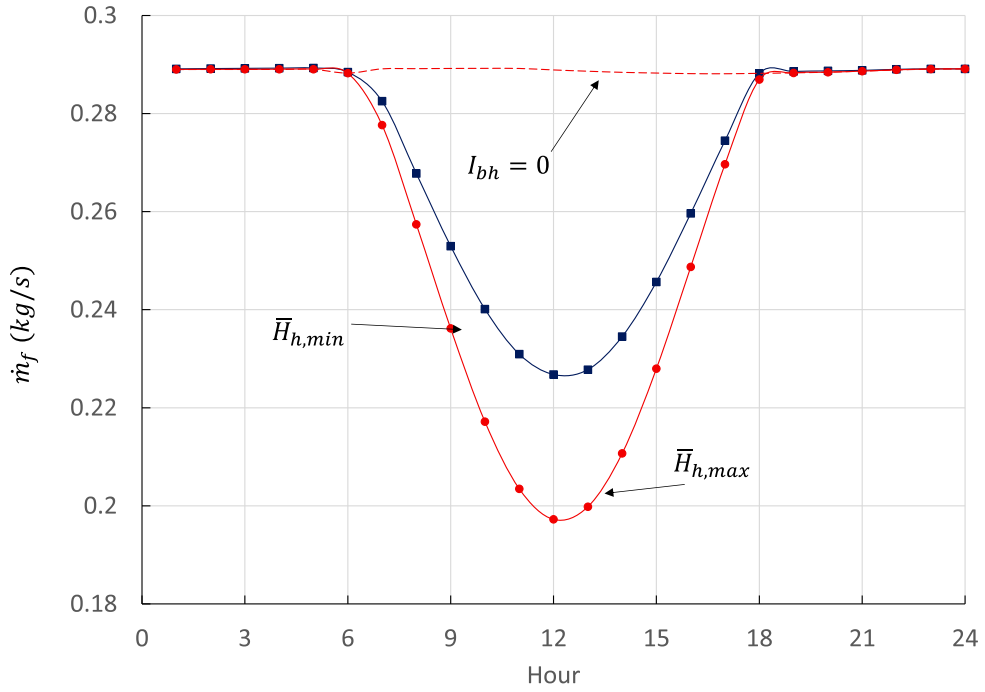

Fig. 18. Daily evolution of global radiation on fuel consumption.

close to the operation point (OP) that occurs when $r_p = 9.9$. Regarding the second case (continuous line), it is possible to observe a decrease in the net output power plant associated with the reduction in the heat exchanger effectiveness. The maximum power point position moves to the left respect the reference case to a value of $r_p = 8.6$.

Fig. 16 shows overall and heat engine efficiencies as a function of different moments during the day. In this case, the same average ambient temperature was used for the three cases, to observe the effect of solar contribution. In this sense, results are obtained for (1) night hours (i.e., when there is not solar contribution), and two specific hours of the day (2) 9 A.M. and (3) noon. Table 4 also presents values of r_p for which η and η_h become the maximum and their respective values. It is observed that the optimum points vary respect the operation point ($r_{p,OP} = 9.9$) and the maximum power point ($r_{p,MO} = 8.6$) through the day. Minimum overall efficiency values are obtained at noon where maximum heat losses are attained, while the behaviour improves as the solar contribution comes nil during the night.

4.2.3. Influence of Barranquilla radiation variation on the CSP plant performance

As indicated in Section 2.1, direct radiation depends on daily average values of diffuse and global radiation in the specific location.

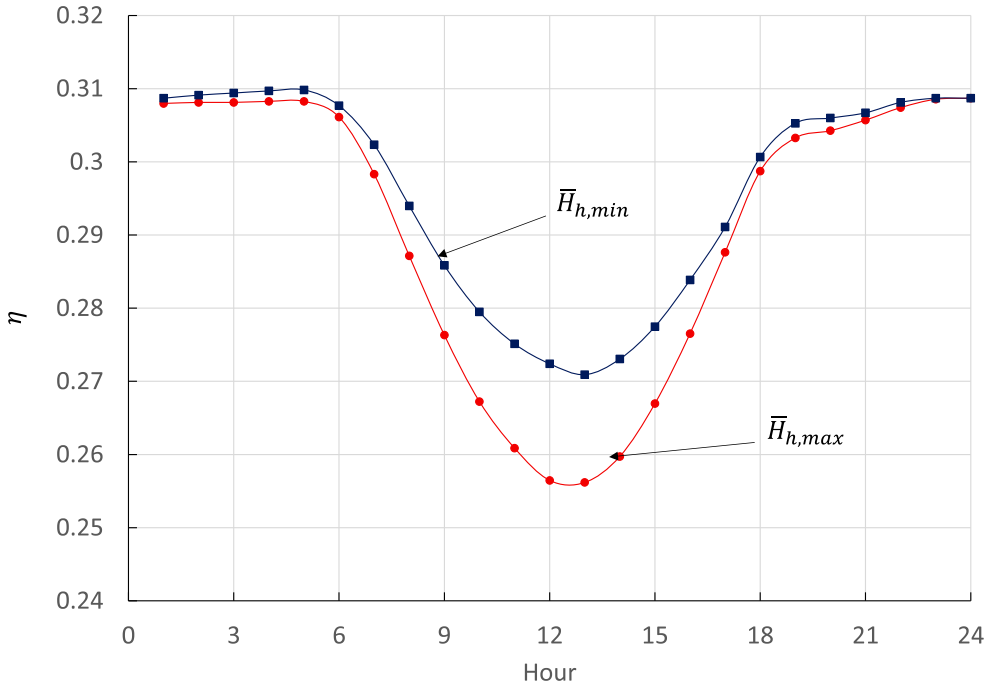

Fig. 19. Influence of global radiation on daily evolution of overall thermal efficiency.

Table 5
Molar fraction, standard chemical exergy and molar mass of natural gas components in Barranquilla.

Component	Molar fraction	Standard chemical exergy [kJ/kmol]	Molar mass [kg/kmol]
CH_4	0.8987	836510	16.43
C_2H_6	0.0587	1504360	30.07
CO_2	0.0178	20140	44.01
C_3H_8	0.0178	2163190	44.097
C_4H_{10}	0.0073	2818930	58.124

The previous results were obtained with the annual mean values of both global and diffuse radiation. In this section, the influence of global radiation on the plant operation is presented and is estimated for the middle day of March ($n = 75$) where the global radiation $\overline{H}_h$ is maximum and for the middle day of November ($n = 315$) when it is minimal. The average ambient temperatures of these two months are also used [72]. Variations in the global radiation have a significant effect on the amount of solar transfer to the working fluid, and then the fuel consumption and the overall plant efficiency. Fig. 17 shows the solar heat fraction transfer to the heat engine, f; as expected, the solar resource variation disturbs the solar fraction. In particular, for the month of lowest radiation, the solar factor decreases by 31.4% at noon for the day of the month with more solar radiation. Fig. 18 shows the daily evolution of fuel consumption for both the global radiation (hybrid conditions) and the plant operating without the solar concentration system ($I_{bh} = 0$). The area between consumption during hybrid operation and the line of operation without the solar system represents fuel savings. The estimated consumption is hourly-averaged to account the radiation variation effect over fuel intake, implying a daily fuel save of 9.21% when $\overline{H}_{h,max}$ and 6.3% when $\overline{H}_{h,min}$). A similar behaviour was estimated for the Solugas plant, where average fuel savings varied between 4% and 11.7% depending on the season [35]. Additionally, the fuel conversion rate, r_e, presents a 12.3% decrease as solar contribution reduce through the day and between both extreme conditions (see Fig. 17) with a relative difference of 0.84%.

Fig. 19 shows the effect of the solar global radiation on the overall plant efficiency. For the day of highest radiation, the relative amplitude of the yield is 20.88%, and for the day of the lowest radiation, it is 14.57%. Additionally, for the moment of the higher radiation (midday), the overall efficiency decreases by 5.8%. Besides, the influence of radiation changes on the solar concentration system efficiency daily evolution can be neglected since it represents a relative difference of 0.84%. As observed, several factors can affect the cycle efficiency; in particular, the pressure ratio presents a significant impact, showing that for the evaluated range, η reduces by 49%. Conversely, when solar radiation is maximum, the efficiency is reduced by 15% regarding the night hours. Meanwhile, for the months of maximum and minimum radiation, the difference in η is only 5%, while the temperature variation hardly varies the efficiency of the cycle by 2.3%.

5. Exergy analysis of the hybrid thermal solar plant

The previous section presented the thermal hybrid solar plant energy analysis under Colombian conditions. In this section, the exergy analysis of the CSP plant is shown. As noted in Section 2.3, exergy destruction is estimated from enthalpy and entropy values at each state within the power cycle and the operating conditions of the solar concentration system. However, evaluation of fuel, air, and combustion gases (including the combustion air excess) exergy is required to determine the exergy destruction of the combustion chamber and the associated heat exchanger.

According to the previous, Table 5 presents natural gas molar composition used to evaluate the molar mass [67] and standard chemical exergy of each component [79]. Fuel specific energy is obtained from Eq. 54, and then divided by the natural gas molar mass $PM_{m,f} = 18.1749059$ kg/kmol, which is average-weighted considering all components [53]. The combustion air exergy is evaluated similarly, by taking air as a reference with a composition 21% of O_2 and 79% of H_2. Regarding the exhaust gases, a combustion analysis was carried out with 300% air excess to ensure complete combustion, leading to $\dot{m}_a = 48.82\dot{m}_f$.

5.1. CSP plant components exergy destruction

Exergy destruction analysis complements the energy study performed in Section 4. Results in this section are for the same hours used

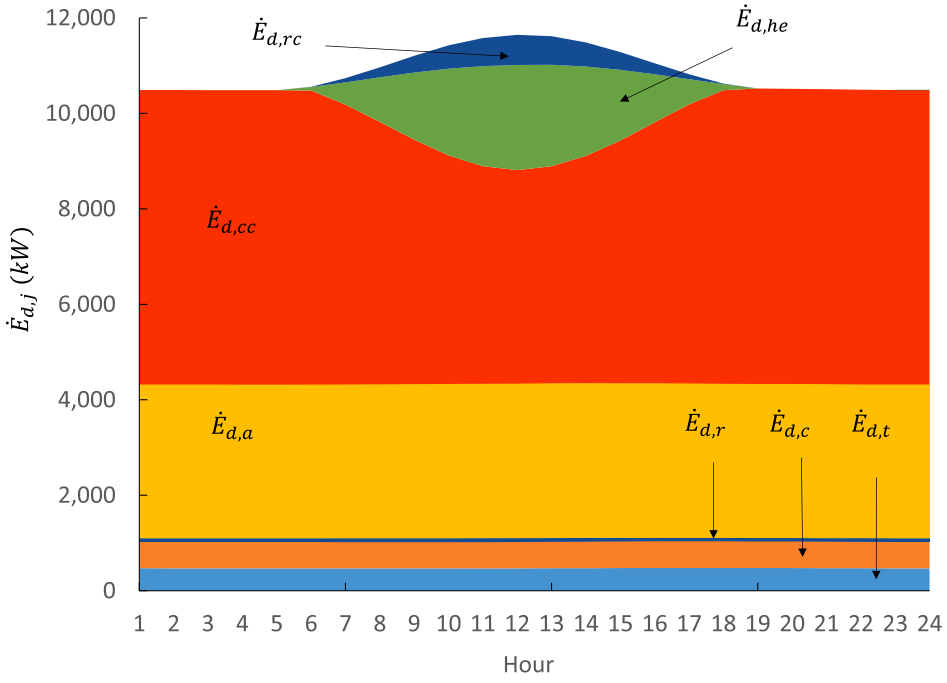

(a)

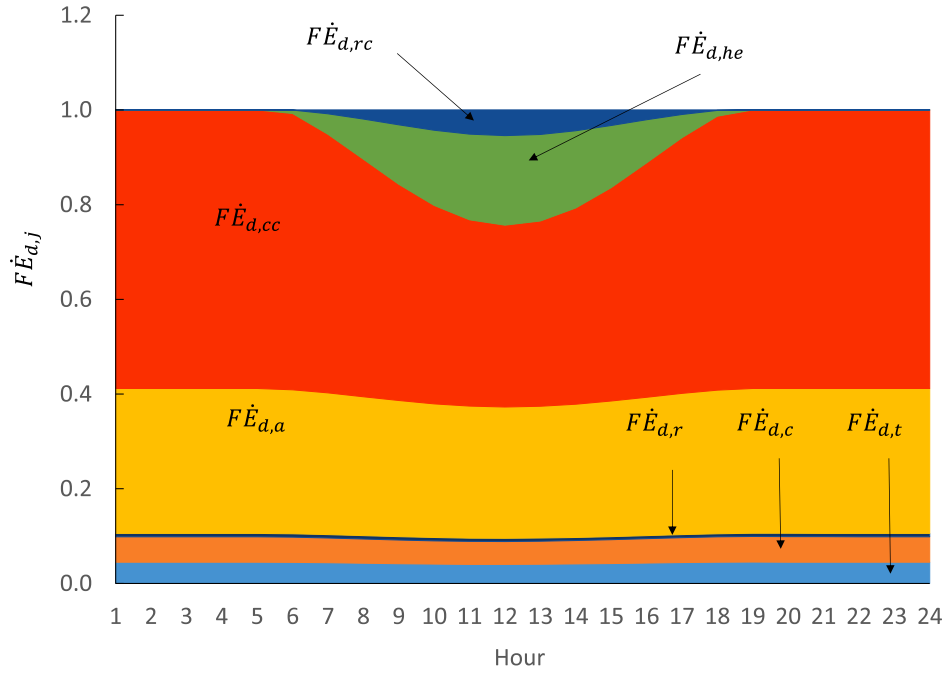

(b)

Fig. 20. Hourly evolution of exergy destruction (a) and exergy destruction fraction (b) of each component.

to estimated direct radiation with the DNI solar model and ambient temperature T_0 (see Fig. 9 and Section 3.2) for the conditions of Barranquilla. Fig. 20a shows hourly exergy destruction of all thermosolar components. It is observed that the maximum exergy destruction occurs at the combustion chamber, $\dot{E_{d,cc}}$, reaching an average value of 6177.08 kW that decreases as fuel consumption is reduced (corresponding to a rise in solar contribution) to a minimum of 4472.78 kW, representing a downward of 27.5%. Available chemical fuel exergy and the elevate temperature of this process are the reasons for such high exergy destruction values. Fig. 20a also shows that the daily evolution of the exergy destruction of solar concentration components increases, as the solar contributions become significant, reaching a maximum value at midday: 2203.23 kW for the heliostat field and 630.99 kW for the solar receiver.

Table 6
Exergy destruction fraction of in each component.

Variable	Night (average)	12 P.M. (noon)
Turbine ($F\dot{E}_{d,t}$)	0.04495	0.04028
Compressor ($F\dot{E}_{d,c}$)	0.05382	0.04823
Regenerator ($F\dot{E}_{d,r}$)	0.0070	0.00685
Atmosphere heat exchanger ($F\dot{E}_{d,a}$)	0.3060	0.2772
Combustion chamber ($F\dot{E}_{d,c}$)	0.5881	0.3840
Heliostat field ($F\dot{E}_{d,he}$)	0	0.1891
Central receiver ($F\dot{E}_{d,rc}$)	0	0.05418

Additionally, Fig. 20b shows the hourly variation of the exergy destruction fraction of the thermosolar plant components. The heliostats field reaches a maximum contribution (18.97%) at noon, while the solar receiver attains a maximum of 5.41% at that moment of the day. The heat exchanger used to release residual heat from the system to its surroundings is the second lager contributor to the exergy destruction component of the plant, with an average of 3218.89 kW. Concerning other parts, the variation of the exergy destruction is smaller, being the regenerator the element that less exergy destroys with an average of 75.28 kW. Table 6 shows values for the exergy destruction fraction for other components of the plant and two different moments during the day. As expected, when the solar concentration system is included, the exergy destruction fraction of the other components reduces at midday.

5.2. Influence of heat exchangers effectiveness on exergy destruction

As was presented before, the heat exchanger associated with the combustion chamber and the one used to release residual heat from the system to its surroundings have an essential effect on the energy performance as well on the exergy destruction of the CSP plant. Following the analysis presented in Section 4.2, the effectiveness of both heat exchangers is settled to 0.94 and 0.98 to account for the effects of this parameter (and compressor and turbine temperatures) on exergy destruction and efficiency throughout the day. Fig. 21a shows that the exergy destruction of the heat exchanger associated with the combustion has an average increase of 7.8% during no solar contribution hours when heat exchanger effectiveness is reduced. In the case of the heat exchanger that transfer heat to the environment, the increase is 8.98% when effectiveness is decreased (see Fig. 21b). Heat exchanger effectiveness variation affects the destruction of exergy of the plant, presenting an average increase of 6.59% during the night and of 4.76% at midday. Reduction of heat exchangers effectiveness leads to an increase in the irreversibilities of the components and therefore, in the exergetic efficiency of the plant, as presented in Fig. 22. Concerning the overall plant and Brayton engine exergy efficiency, a performance reduction of the plant is observed: overall exergy efficiency has an average decrease of 13.32% at night and 11.77% at midday; however, the exergy efficiency of the Brayton heat engine drop is 9.05%.

5.3. Influence of pressure ratio on the exergy efficiency

In this section, the evolution of the overall exergy efficiency during night hours and two specific hours of the day (9 A.M. and 12 P.M) is presented. Fig. 23 shows that exergy efficiencies have similar behaviour to those obtained for the energy analysis (see Fig. 16). It is also observed that the maximum values of efficiency and exergy efficiencies are achieved for similar amounts of the pressure ratio between 5.7 and 6.1 (see Table 7). However, the importance of the overall exergy efficiency η_{ex} are lowered respect to those of the overall efficiency, mainly due to the large amount of exergy destroyed at relevant components such as the combustion chamber and the heat exchanger to the environment. Additionally, around noon, η_{ex} attains its minimum value because of the inlet exergy to the solar concentration system (heliostats field and central receiver) as shown in Fig. 21. Regarding the exergy efficiency of the heat engine η_{exh} this is greater compared with the first law heat engine efficiency η_h, due to the fact that less exergy enters the Brayton heat engine and a smaller amount of exergy for the same power is destroyed.

5.4. Influence of the global radiation in the exergy destruction

Global radiation also has an impact on the exergy destruction of the solar concentration system, according to the proposed model. Fig. 24 shows the exergy destruction evolution when global solar radiation attains its minimum and maximum value (see Section 4.2.3 for the conditions used). An increase in the exergy destruction at the heliostats field around 40.1% and 56.3% at the central tower receiver at midday is observed, with a considerable variation between days of higher and lower radiation. On the other hand, Fig. 25 presents the overall exergy efficiency variation in terms of global radiation. At the moment when solar contribution begins, a decrease in η_{ex} is observed, as is the case of the overall efficiency η (see Fig. 19). In this sense, for the day with higher global radiation, the relative amplitude is 10.3%, and for the day with the minimum value, it is 7.3%. Finally, the influence of the ambient temperature variation trend is also observed on the exergy efficiency, especially during no solar contribution operating conditions.

6. Conclusions

The DNI model used to estimate hourly solar radiation for the Colombian cities, present RMSE (Mean Squared Error) and the MABE (Means Absolute Bias Error) acceptable values according to the literature when was used to predict the global radiation of Seville, validating its use for the study performed in this work. As observed in the results, the city selected to evaluate the performance of a CSP plant under Colombian conditions, presents an average global radiation value similar to the reference case (Seville, Spain), but with a lower variation throughout the year of this variable as well as the ambient temperature.

The thermodynamic models for both energy and exergy analysis had been used to estimate the CSP plant operation at different times of the day, where its accuracy was evaluated by systematically replicating the results of the Solugas plant with an error level acceptable for this kind of predictions. The model also allows different configurations of the plant, such as the use or not of regenerator or hybridization system. That allowed the model to be validated concerning data from a commercial turbine and literature referring to a research and development project that is currently in operation, the results of the validation shown a good fit between the values estimated by the model and the reference data. Results for the CSP power plant, in terms of energy and exergy efficiencies, were evaluated to determine the effect of the selected site and operational conditions on the overall plant performance.

Taking into account that in latitudes such as Colombia, the hours of sunrise and sunset do not vary as much as if it occurs at very high latitudes [35]. Then in hours of available solar resources, the increase in the global radiation augments the solar fraction and therefore reduces fuel consumption. Thus, the influence of irradiation on the solar fraction and fuel consumption is most noticeable. Solar radiation variation affects a smaller proportion of the efficiency of the solar concentration system around noon, being significant near the sunrise and sunset. Additionally, a rise in radiation implies an increase in exergy destruction in both the field of heliostats and the solar receiver, which decreases the exergetic efficiency of the plant. Then, the maximum energy and exergy power values occur at higher-pressure ratios compared with the point of maximum efficiency, which are presented in a range of pressure ratios between 5.7 and 6.4. In contrast, the maximum power of the cycle is given to 8.6.

Results for the operation of the CSP plant under Barranquilla conditions using air as a working fluid present almost constant power values. The implementation of the combustion chamber as a

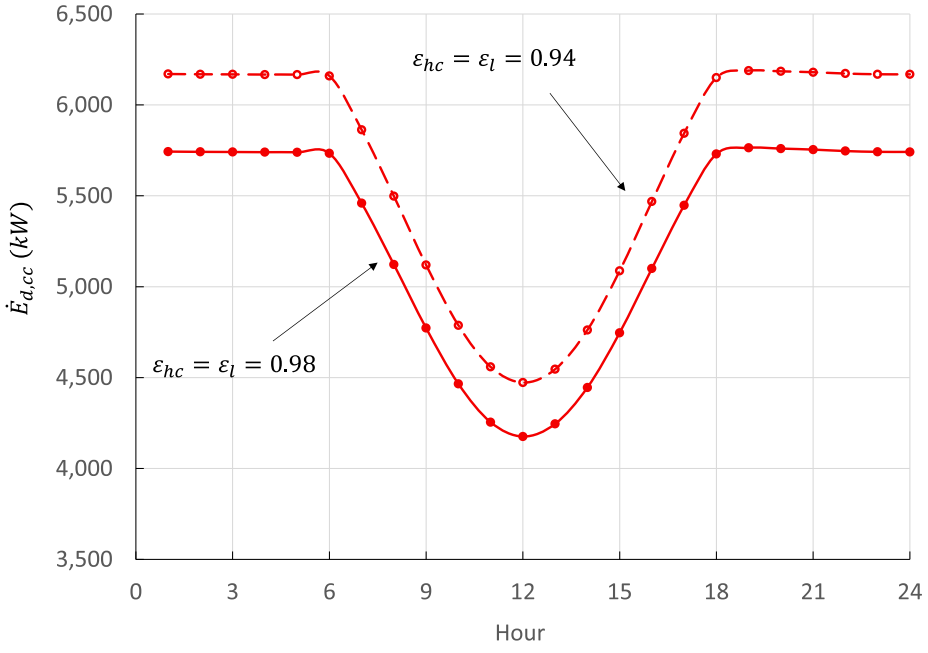

(a)

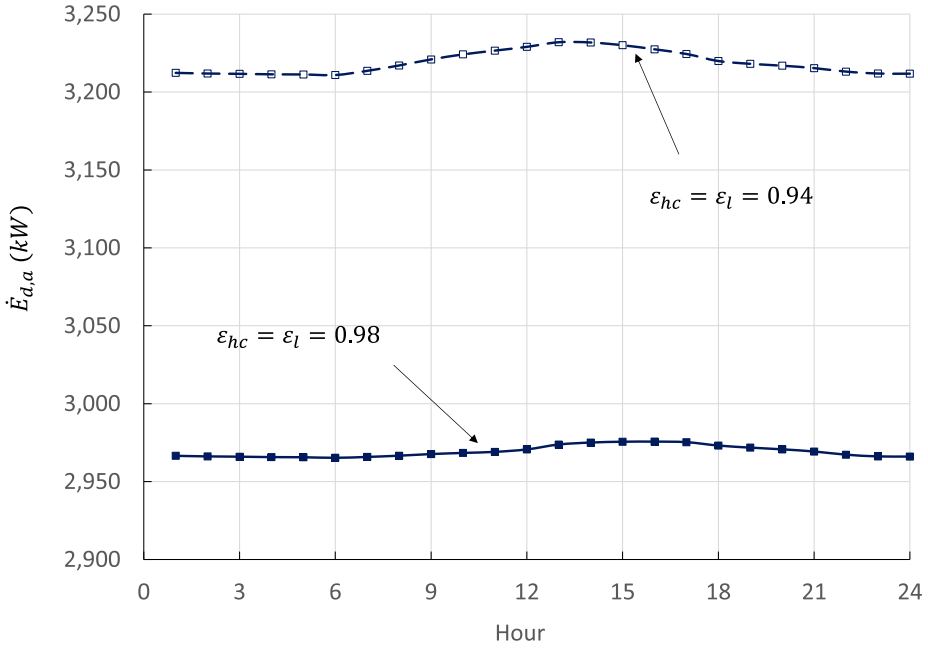

(b)

Fig. 21. Influence on the exergy destruction of heat exchanger effectiveness at combustion chamber (a) and for release heat to ambient (b).

complementary device and the low variation in ambient temperature conducted to a relative amplitude of 4.5%. Additionally, the reduction in the heat exchangers effectiveness associated with the combustion chamber and the heat release to the environment, have a direct effect on the performance of the hybrid solar plant, by reducing power by 12% and overall efficiency in an average of 12.15%. Taking into account the exergy destruction fraction in the combustion chamber which reaches a maximum of 0.58, it is possible to develop a more detailed analysis of said component and evaluate options such as the use of alternative working fluids with different operating temperatures to improve the plant's performance. Additionally, the heliostat field represents a significant exergy destruction fraction at noon, which

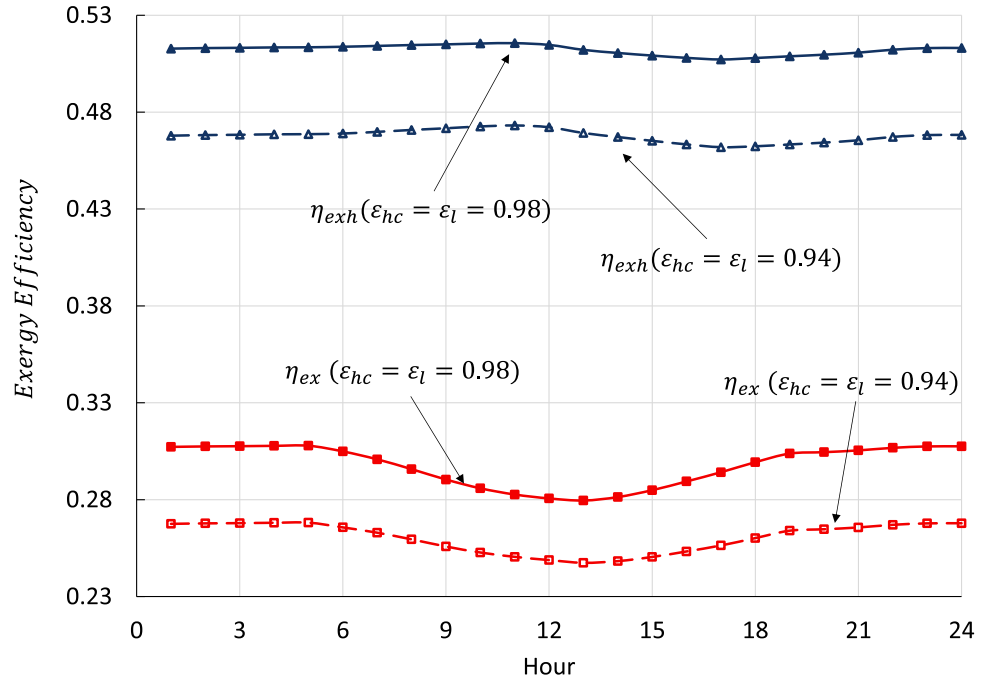

Fig. 22. Variation of the exergy overall plant efficiency and Brayton heat engine as a function of heat exchangers effectiveness.

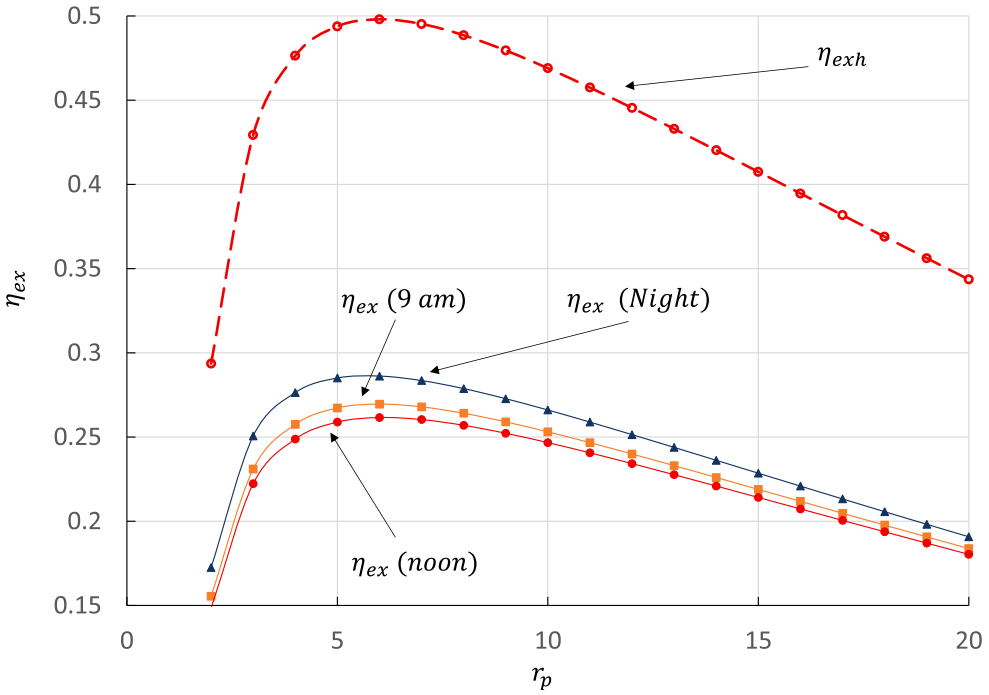

Fig. 23. Influence of the pressure ratio on the on the exergy efficiency.

Table 7
Optimum points of exergy efficiency.

	η_{ex} (night)	η_{ex} (9 A.M.)	η_{ex} (noon)	η_{exh}
r_p	5.7	6	6.1	6
Value	0.2863	0.2695	0.2658	0.4980

opens the way to develop a process for optimizing the size and distribution of the field. Finally, the destruction fraction of exergy in the ambient heat exchanger (≈0.30), encourages the evaluation of a bottoming cycle to take advantage of the heat transfered to the environment. Additionally, it is observed that the Mercury 50 turbine operates near its maximum power point, as seen in Fig. 15.

In the end, the performance of the CSP plant under Colombian conditions presents a similar trend the behaviour reported for the only know operative hybrid thermosolar plant in operation with a Brayton cycle at the scale of MW. This supports the hypothesis that optimized CSP plants in union with traditional fossil thermal cycles can be used to produce energy in Colombia, decreasing dependence on fossil fuel and the associated environmental impact.

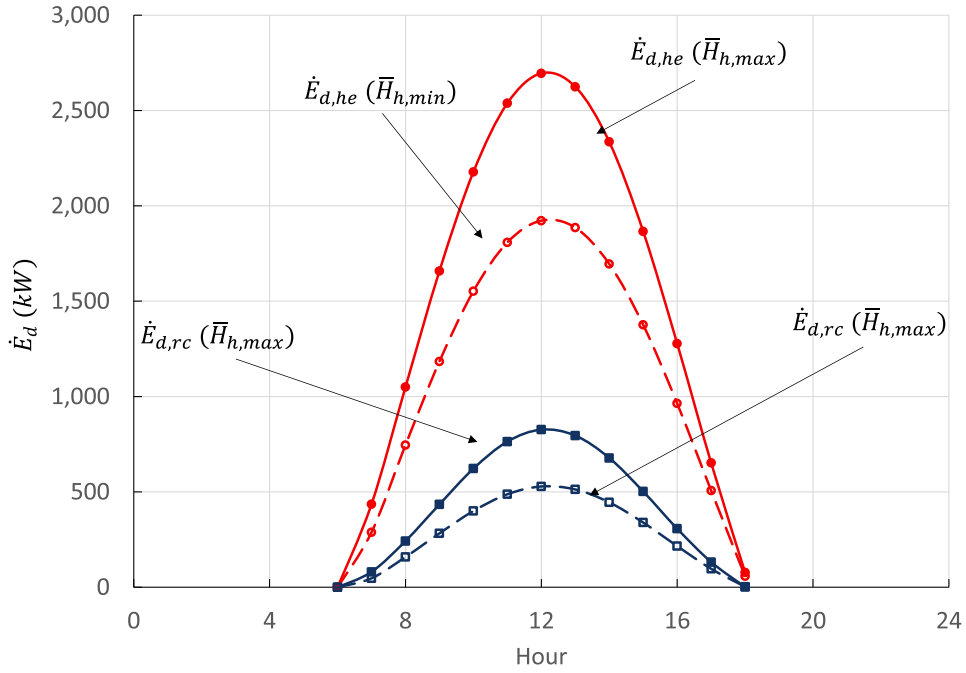

Fig. 24. Influence of global radiation on the exergy destruction of the solar receiver.

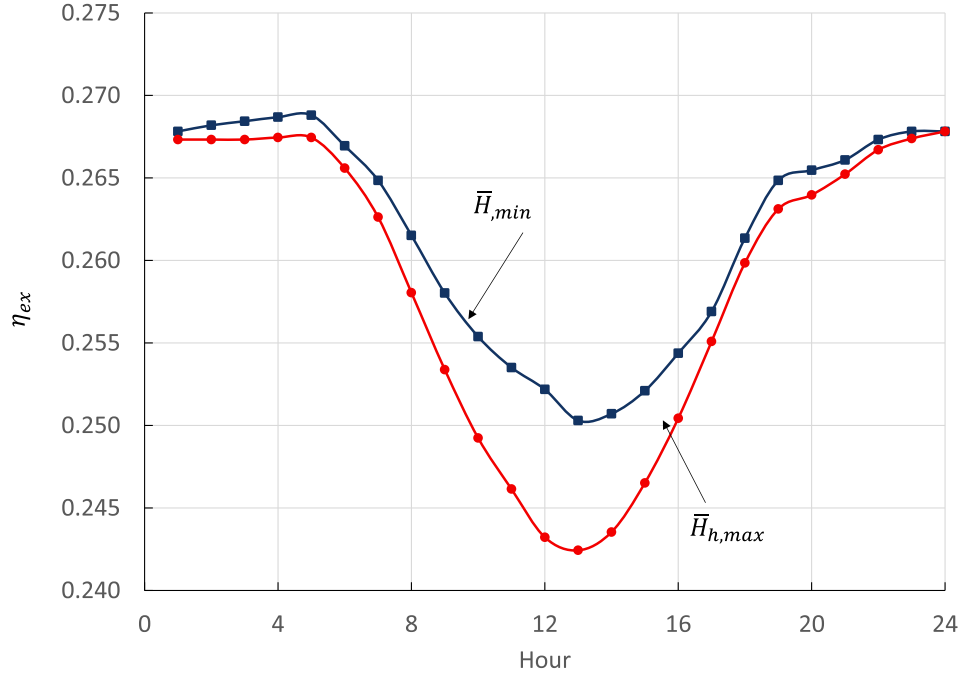

Fig. 25. Influence of global radiation on daily overall exergy efficiency.

CRediT authorship contribution statement

Faustino Moreno-Gamboa: Writing - original draft, Investigation, Software. **Ana Escudero-Atehortua:** Writing - review & editing, Formal analysis. **César Nieto-Londoño:** Writing - review & editing, Conceptualization, Supervision.

Declaration of Competing Interest

The authors declare that they have no known competing financial interests or personal relationships that could have appeared to influence the work reported in this paper.

Acknowledgments

The first author acknowledges to Francisco de Paula Santander University and Colciencias for his Doctoral scholarship.

References

[1] DNP, Energy demand situation in Colombia, Tech. rep., Departamento Nacional de Planeación, 2017.
[2] UPME, Plan energético nacional 2020–2050, Tech. rep., Unidad de Planeación Minero Energética, 2019.
[3] DNP, Energy supply situation in Colombia, Tech. rep., Departamento Nacional de Planeación, 2017.
[4] UPME, Plan de expansión de referencia generación transmisión 2015–2029, Tech.

rep., Unidad de Planeación Minero Energética, 2015.
[5] DNP, Green growth policy proposals, Tech. rep., Departamento Nacional de Planeación, 2018.
[6] REN21, Renewables 2018 global status report. a comprehensive annual overview of the state of renewable energy, Tech. Rep. GSR2018, REN21 Secretariat, Paris, 2018.
[7] T. Bouhal, Y. Agrouaz, T. Kousksou, A. Allouhi, T.E. Rhafiki, A. Jamil, M. Bakkas, Technical feasibility of a sustainable concentrated solar power in morocco through an energy analysis, Renew. Sustain. Energy Rev. 81 (2018) 1087–1095.
[8] M.M. Rafique, H.M.S. Bahaidarah, Thermo-economic and environmental feasibility of a solar power plant as a renewable and green source of electrification, Int. J. Green Energy 16 (15) (2019) 1577–1590.
[9] M.Z. Jacobson, M.A. Delucchi, Providing all global energy with wind, water, and solar power, part i: technologies, energy resources, quantities and areas of infrastructure, and materials, Energy Policy 39 (3) (2011) 1154–1169.
[10] W. Le Roux, T. Bello-Ochende, J. Meyer, A review on the thermodynamic optimisation and modelling of the solar thermal brayton cycle, Renew. Sustain. Energy Rev. 28 (2013) 677–690.
[11] L. Ding, A. Akbarzadeh, B. Singh, M. Remeli, Feasibility of electrical power generation using thermoelectric modules via solar pond heat extraction, Energy Convers. Manage. 135 (2017) 74–83.
[12] I. Elsayed, Y. Nishi, A feasibility study on power generation from solar thermal wind tower: inclusive impact assessment concerning environmental and economic costs, Energies 11 (11) (2018) 3181.
[13] S. Kirmani, M. Jamil, I. Akhtar, Economic feasibility of hybrid energy generation with reduced carbon emission, IET Renew. Power Gen. 12 (8) (2018) 934–942.
[14] M. Santos, C. Miguel-Barbero, R. Merchán, A. Medina, A. Calvo Hernández, Roads to improve the performance of hybrid thermosolar gas turbine power plants: Working fluids and multi-stage configurations, Energy Convers. Manage. 165 (2018) 578–592.
[15] N. Suresh, N. Thirumalai, S. Dasappa, Modeling and analysis of solar thermal and biomass hybrid power plants, Appl. Therm. Eng. 160 (2019) 114121.
[16] N. Taylor, Solar thermal electricity: technology development report, Tech. rep.
[17] H. Jouhara, A. Żabnieńska Góra, N. Khordehgah, D. Ahmad, T. Lipinski, Latent thermal energy storage technologies and applications: a review, Int. J. Thermofluids (2020) 100039.
[18] H. Jouhara, N. Khordehgah, S. Almahmoud, B. Delpech, A. Chauhan, S.A. Tassou, Waste heat recovery technologies and applications, Therm. Sci. Eng. Prog. 6 (2018) 268–289.
[19] Z. Liu, Y. Yan, R. Fu, M. Alsaady, Enhancement of solar energy collection with magnetic nanofluids, Therm. Sci. Eng. Prog. 8 (2018) 130–135.
[20] E. Bernardos, I. López, J. Rodríguez, A. Abánades, Assessing the potential of hybrid fossil–solar thermal plants for energy policy making: brayton cycles, Energy Policy 62 (2013) 99–106.
[21] C. Soares, Gas Turbines: A Handbook of Air, Land and Sea Applications, Butterworth-Heinemann, 2012.
[22] M. Jamel, A.A. Rahman, A. Shamsuddin, Advances in the integration of solar thermal energy with conventional and non-conventional power plants, Renew. Sustain. Energy Rev. 20 (2013) 71–81.
[23] M.T. Dunham, B.D. Iverson, High-efficiency thermodynamic power cycles for concentrated solar power systems, Renew. Sustain. Energy Rev. 30 (2014) 758–770.
[24] J.W. Teets, J.M. Teets, A 150Kw Integrated Solar Combined Cycle (ISCC) power plant volume 8: energy systems: analysis, thermodynamics and sustainability, Sustain. Prod. Process. (2008) 321–331.
[25] M.U. Sajid, Y. Bicer, Thermodynamic assessment of chemical looping combustion and solar thermal methane cracking-based integrated system for green ammonia production, Therm. Sci. Eng. Prog. 19 (2020) 100588.
[26] H. Nakatani, T. Osada, Development of a concentrated solar power generation system with a hot-air turbine, Mitsubishi Heavy... 49 (1) (2012) 1–5.
[27] S. Kim, M.S. Kim, M. Kim, Parametric study and optimisation of closed brayton power cycle considering the charge amount of working fluid, Energy 198 (2020) 117353.
[28] F. Calise, M.D. d'Accadia, L. Libertini, M. Vicidomini, Thermoeconomic analysis of an integrated solar combined cycle power plant, Energy Convers. Manage. 171 (2018) 1038–1051.
[29] J. Spelling, D. Favrat, A. Martin, G. Augsburger, Thermoeconomic optimization of a combined-cycle solar tower power plant, Energy 41 (1) (2012) 113–120, 23rd International Conference on Efficiency, Cost, Optimization, Simulation and Environmental Impact of Energy Systems, ECOS 2010.
[30] I.A. Ehtiwesh, M.C. Coelho, A.C. Sousa, Exergetic and environmental life cycle assessment analysis of concentrated solar power plants, Renew. Sustain. Energy Rev. 56 (2016) 145–155.
[31] R. Merchán, M. Santos, I. Reyes-Ramírez, A. Medina, A. Calvo Hernández, Modeling hybrid solar gas-turbine power plants: thermodynamic projection of annual performance and emissions, Energy Convers. Manage. 134 (2017) 314–326.
[32] R. Merchán, M. Santos, I. Heras, J. Gonzalez-Ayala, A. Medina, A.C. Hernández, On-design pre-optimization and off-design analysis of hybrid brayton thermosolar tower power plants for different fluids and plant configurations, Renew. Sustain. Energy Rev. 119 (2020) 109590.
[33] D. Olivenza-León, A. Medina, A. Calvo Hernández, Thermodynamic modeling of a hybrid solar gas-turbine power plant, Energy Convers. Manage. 93 (2015) 435–447.
[34] O. Behar, Solar thermal power plants – a review of configurations and performance comparison, Renew. Sustain. Energy Rev. 92 (2018) 608–627.
[35] M. Santos, R. Merchán, A. Medina, A. Calvo Hernández, Seasonal thermodynamic prediction of the performance of a hybrid solar gas-turbine power plant, Energy Convers. Manage. 115 (2016) 89–102.
[36] S. Sánchez, Modelización, análisis y optimización termodinámica de plantas de potencia multietapa tipo Brayton. Aplicación a centrales termosolares, Ph.D. thesis, Universidad de Salamanca, 2012.
[37] J. Kim, J.-S. Kim, W. Stein, Simplified heat loss model for central tower solar receiver, Solar Energy 116 (2015) 314–322.
[38] Y. Zhang, B. Lin, J. Chen, Optimum performance characteristics of an irreversible solar-driven brayton heat engine at the maximum overall efficiency, Renew. Energy 32 (5) (2007) 856–867.
[39] B. Sahin, A. Kodal, T. Yilmaz, H. Yavuz, Maximum power density analysis of an irreversible joule - brayton engine, J. Phys. D Appl. Phys. 29 (5) (1996) 1162–1167.
[40] V. Ferraro, V. Marinelli, An evaluation of thermodynamic solar plants with cylindrical parabolic collectors and air turbine engines with open joule–brayton cycle, Energy 44 (1) (2012) 862–869, Integration and Energy System Engineering, European Symposium on Computer-Aided Process Engineering 2011.
[41] Z. Liao, A. Faghri, Thermal analysis of a heat pipe solar central receiver for concentrated solar power tower, Appl. Therm. Eng. 102 (2016) 952–960.
[42] V. Ferraro, F. Imineo, V. Marinelli, An improved model to evaluate thermodynamic solar plants with cylindrical parabolic collectors and air turbine engines in open joule–brayton cycle, Energy 53 (2013) 323–331.
[43] C.K. Ho, B.D. Iverson, Review of high-temperature central receiver designs for concentrating solar power, Renew. Sustain. Energy Rev. 29 (2014) 835–846.
[44] W. Le Roux, T. Bello-Ochende, J. Meyer, Operating conditions of an open and direct solar thermal brayton cycle with optimised cavity receiver and recuperator, Energy 36 (10) (2011) 6027–6036.
[45] C. Tang, H. Feng, L. Chen, W. Wang, Power density analysis and multi-objective optimisation for a modified endoreversible simple closed brayton cycle with one isothermal heating process, Energy Rep. 6 (2020) 1648–1657.
[46] J.H. Park, H.S. Park, J.G. Kwon, T.H. Kim, M.H. Kim, Optimization and thermodynamic analysis of supercritical CO2 brayton recompression cycle for various small modular reactors, Energy 160 (2018) 520–535.
[47] D. Thanganadar, F. Asfand, K. Patchigolla, Thermal performance and economic analysis of supercritical carbon dioxide cycles in combined cycle power plant, Appl. Energy 255 (2019) 113826.
[48] M. Ashouri, M.H. Ahmadi, S.M. Pourkiaei, F.R. Astaraei, R. Ghasempour, T. Ming, J.H. Hemati, Exergy and exergo-economic analysis and optimization of a solar double pressure organic rankine cycle, Therm. Sci. Eng. Prog. 6 (2018) 72–86.
[49] H. Zhai, Y. Dai, J. Wu, R. Wang, Energy and exergy analyses on a novel hybrid solar heating, cooling and power generation system for remote areas, Appl. Energy 86 (9) (2009) 1395–1404.
[50] V. Zare, M. Hasanzadeh, Energy and exergy analysis of a closed brayton cycle-based combined cycle for solar power tower plants, Energy Convers. Manage. 128 (2016) 227–237.
[51] M. Atif, F.A. Al-Sulaiman, Energy and exergy analyses of solar tower power plant driven supercritical carbon dioxide recompression cycles for six different locations, Renew. Sustain. Energy Rev. 68 (2017) 153–167.
[52] M.H. Ahmadi, M. Mehrpooya, S. Abbasi, F. Pourfayaz, J.C. Bruno, Thermo-economic analysis and multi-objective optimization of a transcritical CO2 power cycle driven by solar energy and lng cold recovery, Therm. Sci. Eng. Prog. 4 (2017) 185–196.
[53] T. Yue, N. Lior, Thermal hybrid power systems using multiple heat sources of different temperature: thermodynamic analysis for brayton cycles, Energy 165 (2018) 639–665.
[54] M. Abid, M.S. Khan, T.A.H. Ratlamwala, Comparative energy, exergy and exergo-economic analysis of solar driven supercritical carbon dioxide power and hydrogen generation cycle, Int. J. Hydrogen Energy 45 (9) (2020) 5653–5667, iEEES-10 – International Exergy, Energy and Environment Symposium.
[55] Modelica, 2019. http://www.modelica.org.
[56] DYMOLA Systems Engineering, 2019. URL http://www.dynasim.se.
[57] C. Gueymard, Prediction and performance assessment of mean hourly global radiation, Solar Energy 68 (3) (2000) 285–303.
[58] D.Y. Goswami, Principles of Solar Engineering, third ed., CRC Press, 2015.
[59] B.Y. Liu, R.C. Jordan, The interrelationship and characteristic distribution of direct, diffuse and total solar radiation, Solar Energy 4 (3) (1960) 1–19.
[60] R. Mejdoul, M. Taqi, The mean hourly global radiation prediction models investigation in two different climate regions in Morocco, Int. J. Renew. Energy Res. 2 (4) (2012) 608–617.
[61] W. Yao, Z. Li, T. Xiu, Y. Lu, X. Li, New decomposition models to estimate hourly global solar radiation from the daily value, Solar Energy 120 (2015) 87–99.
[62] J. Chandrasekaran, S. Kumar, Hourly diffuse fraction correlation at a tropical location, Solar Energy 53 (6) (1994) 505–510.
[63] N. Aeronautics, S. Administration, Power Data Access Viewer (2018). https://power.larc.nasa.gov/data-access-viewer/.
[64] M. Romero, R. Buck, J.E. Pacheco, An update on solar central receiver systems, projects, and technologies, J. Solar Energy Eng. 124 (2) (2002) 98–108.
[65] J.A. Duffie, W.A. Beckman, Solar Engineering of Thermal Processes, John Wiley & Sons, 2013.
[66] W. Wang, L. Chen, F. Sun, C. Wu, Performance analysis for an irreversible variable temperature heat reservoir closed intercooled regenerated brayton cycle, Energy Convers. Manage. 44 (17) (2003) 2713–2732.
[67] Y. Çengel, M. Boles, Thermodynamic: An Engineering Approach, eighth ed., McGraw-Hill, 2015.
[68] D. Kulshreshtha, S. Mehta, Exergy analysis of a regenerative micro gas turbine engine, in: ICFD 10: Tenth International Congress of Fluid Dynamics, 2010.
[69] J. Parrott, Theoretical upper limit to the conversion efficiency of solar energy, Solar Energy 21 (3) (1978) 227–229.
[70] R. Petela, Exergy of undiluted thermal radiation, Solar Energy 74 (6) (2003) 469–488.

[71] Meteosevilla, 2017. URL www.meteosevilla.com.
[72] E. Ramírez-Cerpa, M. Acosta-Coll, J. Vélez-Zapata, Análisis de condiciones climatológicas de precipitaciones de corto plazo en zonas urbanas: caso de estudio Barranquilla, Colombia, Idesia (Arica) 35 (ahead) (2017) 0–0. doi:10.4067/S0718-34292017005000023.
[73] R. Korzynietz, J. Brioso, A. del Río, M. Quero, M. Gallas, R. Uhlig, M. Ebert, R. Buck, D. Teraji, Solugas – comprehensive analysis of the solar hybrid brayton plant, Solar Energy 135 (2016) 578–589.
[74] P.G. Package, Mercury 50 – Power Generation Packages, Solar Turbines, 2019. https://www.solarturbines.com/en_US/products/power-generation-packages/mercury-50.html.
[75] L. Wu, G. Lin, J. Chen, Parametric optimization of a solar-driven braysson heat engine with variable heat capacity of the working fluid and radiation–convection heat losses, Renew. Energy 35 (1) (2010) 95–100.
[76] A. Romier, Small gas turbine technology, Appl. Therm. Eng. 24 (11) (2004) 1709–1723, Industrial Gas Turbine Technologies.
[77] G. Barigozzi, A. Perdichizzi, C. Gritti, I. Guaiatelli, Techno-economic analysis of gas turbine inlet air cooling for combined cycle power plant for different climatic conditions, Appl. Therm. Eng. 82 (2015) 57–67.
[78] P.E.B. de Mello, D.B. Monteiro, Thermodynamic study of an efgt (externally fired gas turbine) cycle with one detailed model for the ceramic heat exchanger, Energy 45 (1) (2012) 497–502, The 24th International Conference on Efficiency, Cost, Optimization, Simulation and Environmental Impact of Energy, ECOS 2011.
[79] T. Kotas, The Exergy Method of Thermal Plant Analysis, Butterworth-Heinemann, 1985.